PRIMARY RESEARCH ARTICLE

Global Change Biology WILEY

Understanding water and energy fluxes in the Amazonia: Lessons from an observation-model intercomparison

Natalia Restrepo-Coupe[1,2] | Loren P. Albert[1,3] | Marcos Longo[4,5] | Ian Baker[6] | Naomi M. Levine[4,7] | Lina M. Mercado[8,9] | Alessandro C. da Araujo[10,11] | Bradley O'Donnell Christoffersen[12,13] | Marcos H. Costa[14] | David R. Fitzjarrald[15] | David Galbraith[16] | Hewlley Imbuzeiro[14] | Yadvinder Malhi[17] | Celso von Randow[18] | Xubin Zeng[19] | Paul Moorcroft[5] | Scott R. Saleska[1]

[1]Department of Ecology and Evolutionary Biology, University of Arizona, Tucson, AZ, USA

[2]School of Life Sciences, University of Technology Sydney, Ultimo, NSW, Australia

[3]Biology Department, West Virginia University, Morgantown, WV, USA

[4]Department of Organismic and Evolutionary Biology, Harvard University, Cambridge, MA, USA

[5]Jet Propulsion Laboratory, California Institute of Technology, Pasadena, CA, USA

[6]Colorado State University, Atmospheric Science, Fort Collins, CO, USA

[7]College of Letters, Arts, and Science, University of Southern California, Los Angeles, CA, USA

[8]University of Exeter, College of Life and Environmental Sciences, Exeter, Devon, UK

[9]Centre for Ecology and Hydrology, Wallingford, Oxfordshire, UK

[10]Embrapa Amazônia Oriental, Belém, Pará, Brazil

[11]Programa LBA, Instituto Nacional de Pesquisas da Amazônia (INPA), Manaus, Amazonas, Brazil

[12]Department of Biology, University of Texas Rio Grande Valley, Edinburg, TX, USA

[13]Earth and Environmental Sciences Division, Los Alamos National Laboratory, Los Alamos, NM, USA

[14]Department of Agricultural Engineering, Federal University of Vicosa, Vicosa, Mato Grosso, Brazil

[15]University at Albany SUNY, Albany, NY, USA

[16]School of Geography, University of Leeds, Leeds, UK

[17]Environmental Change Institute, School of Geography and the Environment, University of Oxford, Oxford, UK

[18]National Institute for Space Research (INPE), Center for Earth Systems Science, São José dos Campos, São Pablo, Brazil

[19]Department of Hydrology and Atmospheric Sciences, University of Arizona, Tucson, AZ, USA

Correspondence
Natalia Restrepo-Coupe, Cupoazu LLC.
Email: nataliacoupe@gmail.com

Abstract

Tropical forests are an important part of global water and energy cycles, but the mechanisms that drive seasonality of their land-atmosphere exchanges have proven challenging to capture in models. Here, we (1) report the seasonality of fluxes of latent heat (LE), sensible heat (H), and outgoing short and longwave radiation at four diverse tropical forest sites across Amazonia—along the equator from the Caxiuanã and Tapajós National Forests in the eastern Amazon to a forest near Manaus, and from the equatorial zone to the southern forest in Reserva Jaru; (2) investigate how vegetation and climate influence these fluxes; and (3) evaluate land surface model performance by comparing simulations to observations. We found that previously identified failure of models to capture observed dry-season increases in evapotranspiration (ET) was

associated with model overestimations of (1) magnitude and seasonality of Bowen ratios (relative to aseasonal observations in which sensible was only 20%–30% of the latent heat flux) indicating model exaggerated water limitation, (2) canopy emissivity and reflectance (albedo was only 10%–15% of incoming solar radiation, compared to 0.15%–0.22% simulated), and (3) vegetation temperatures (due to underestimation of dry-season ET and associated cooling). These partially compensating model-observation discrepancies (e.g., higher temperatures expected from excess Bowen ratios were partially ameliorated by brighter leaves and more interception/evaporation) significantly biased seasonal model estimates of net radiation (R_n), the key driver of water and energy fluxes (LE ~ 0.6 R_n and H ~ 0.15 R_n), though these biases varied among sites and models. A better representation of energy-related parameters associated with dynamic phenology (e.g., leaf optical properties, canopy interception, and skin temperature) could improve simulations and benchmarking of current vegetation–atmosphere exchange and reduce uncertainty of regional and global biogeochemical models.

1 | INTRODUCTION

Tropical forests play a major role in the global water and energy cycles, and modulate tropical atmospheric circulation processes, cloud formation, and precipitation (Hagos & Leung, 2011; Held & Soden, 2006; Jasechko et al., 2013; Silva Dias et al., 2002; Wei et al., 2017; Worden et al., 2007). Water and energy fluxes are intrinsically linked, as energy is required for the phase transition from liquid to vapor. Tropical forests evapotranspire the energy equivalent of more than half of the total solar energy absorbed by earth's land surfaces (Trenberth et al., 2009), helping to maintain high atmospheric water content, increase moisture recycling, and mediate cloud development (Peters, 2016; Tan et al., 2019). Evapotranspiration (ET) mitigates heating as part of the incoming radiation is primarily "consumed" as latent heat (LE) rather than as sensible heat flux (H). High ET rates can offset the warming effect associated with tropical forest low albedo (the ratio of reflected to incoming shortwave radiation, SW_{out}/SW_{down}) driven by its relatively dark surface (Bonan, 2008; Yanagi & Costa, 2011). Therefore, land use change, fire, climate and extreme weather events (Aragão et al., 2007, 2008; Chagnon & Bras, 2005; Davidson et al., 2012) are listed as key factors determining subsequent changes in tropical forest albedos (negative climate forcing) and alterations in the evaporative cooling flux (positive feedbacks—reducing warming; Bonan, 2008; Li et al., 2015; Liu et al., 2019). Measuring and understanding water, radiation, and energy seasonal fluxes under present climatological conditions is thus needed to forecast the future of tropical forests and global atmospheric cycles (Fu et al., 2013; Sena et al., 2018; Spracklen et al., 2018).

Land surface models (LSMs) represent our mechanistic understanding of cause–effect relationships between the surface and the atmosphere and constitute ideal tools to forecast water, energy, and other biogeochemical fluxes (Pitman, 2003). However, given that ecosystem characteristics are diverse and that land–climate interactions are heterogeneous and complex, it is not surprising that LSMs have difficulty in reproducing the seasonality of rainforest ET (Baker et al., 2008; Christoffersen et al., 2014; Costa et al., 2010; Fisher et al., 2014; Restrepo-Coupe et al., 2017). A consistent problem is that models simulate reductions in ET during the dry season (when precipitation is less than ~100 mm month^{-1}), when most observations from eddy covariance (EC) towers in Amazonia show no reductions or even increases in LE, consistent with control by the availability of energy (net radiation), and inconsistent with limitation by available water (Baker et al., 2008; Christoffersen et al., 2014; Costa et al., 2010; Fisher et al., 2007; Restrepo-Coupe et al., 2017; Shuttleworth, 1988).

Previous attempts to improve the dry-season LE discrepancies between LSM simulations and observations of tropical forests have been focused on the parameterization of higher soil water holding capacity, hydraulic redistribution (vegetation control mechanisms), deeper roots that can access the lower soil layers and/or increase root mass (enhanced pathways) and dynamics of stem-water storage (plant hydraulics; Baker et al., 2008; Christoffersen et al., 2014; Harper et al., 2010; Lee et al., 2005; Yan et al., 2020). Unfortunately, some of these model modifications appear to drive LSMs to (1) overestimate annual and/or dry-season ET and/or (2) model simulations could become insensitive to drought conditions.

Christoffersen et al. (2014) previously analyzed simulations from the same model-data intercomparison investigated here, focusing on modeled mechanisms of water supply (rooting depth, access to groundwater sources, and soil water availability) and vegetation demand (intrinsic water use efficiency [iWUE] and stomatal conductance) that drive the simulated dry-season reductions in ET. Chirstoffersen et al. (2014) identified model underrepresentation of phenological processes (including leaf development and associated changes in iWUE) as a cause of the bias. When these same LSM simulations were evaluated for their ability to represent the seasonal dynamics of carbon fluxes in these same tropical forests (Restrepo-Coupe et al., 2017), the analysis found that although water limitation was represented in models as the primary driver of the seasonality of photosynthesis across Amazonia, the LSMs did not accurately represent that seasonality. Observations showed incoming radiation and phenological cycles that included allocation lags between wood, leaf, and nonstructural carbon, and light harvesting adaptations (e.g., leaf demography) dominated carbon exchange and in some instances, were not well represented in LSMs. Both carbon and water fluxes are significantly influenced by tropical forest phenology (Chen et al., 2020; Restrepo-Coupe et al., 2017). However, the relationship between vegetation seasonal cycles and the radiation and energy exchange is not well documented.

Here, we extend the prior work of Christoffersen et al. (2014) and Restrepo-Coupe et al., (2017), building on the consistent finding that LE appears to be controlled by net radiation (R_n). If this finding is correct, then inherent in the challenge of accurate modeling of ET (equivalent LE) is the accurate simulation of the other radiation components (LW_{out} and SW_{out}), as well as the accurate partitioning of the relevant energy fluxes (e.g., energy allocated to LE and H; Bony et al., 2013; Getirana et al., 2014; Longo, Knox, Levine, et al., 2019), in addition to the accurate representation of phenological attributes (e.g., leaf-age driving seasonal canopy conductance values; Lin et al., 2015; Medlyn et al., 2011; see Figure 1). Yet, in tropical forests and across Amazonia there is scarce information on the seasonal cycle of energy-relevant components H, albedo (α), emissivity (ε_s), the Bowen

ratio (Bowen = H/LE), and the outgoing and incoming longwave radiation (LW_{out} and LW_{down}).

Focusing on energy dynamics, we compare forest characteristics and water and energy fluxes from EC and meteorological observations at four tropical forest sites from the Brasil flux network, three Amazonian forests close to the Amazon river (Manaus-K34, Tapajós-K67, and Caxiuanã-CAX) and one southern location (Reserva Jaru-RJA) to four state-of-the-art LSMs (IBIS, ED2, JULES, and CLM3.5; Restrepo-Coupe et al., 2017). The aim of this work is threefold: (1) to quantify and characterize the seasonal fluxes (timing and amplitude) and surface properties of the different water, energy, and radiation cycle components; (2) to determine the relationships between these energy-related fluxes and vegetation and climate drivers, as we investigate the ability of other simple models and relations to predict ecosystem-level fluxes (e.g., linear regressions between R_n and LE); and (3) to identify areas to refine current LSM model formulations and to enhance seasonal LE, H, and R_n simulations by including vegetation characteristics (e.g., albedo) in the analysis and improving the derivation of radiative fluxes (e.g., outgoing SW and LW), with special attention to the inherent coupling of carbon, energy, and water cycles (Figure 1).

2 | METHODS

2.1 | Site descriptions

Data were obtained at four EC flux tower tropical forest locations (Figure 2). All sites were established by the Brazilian-led Large-Scale Biosphere-Atmosphere Experiment in Amazonia (LBA-ECO; Keller et al., 2004) and members of the Brasil flux network (Restrepo-Coupe et al., 2013; da Rocha et al., 2004). Three EC stations comprise a longitudinal transect close to the equator (~3°S) along the Amazon river from east to west, from high to low mean annual net radiation (Figure 2) and different seasonal patterns of monthly precipitation: Caxiuanã (CAX), the Tapajós National forest near Santarém (K67), and the Reserva Cuieiras near Manaus (K34). The fourth site, the
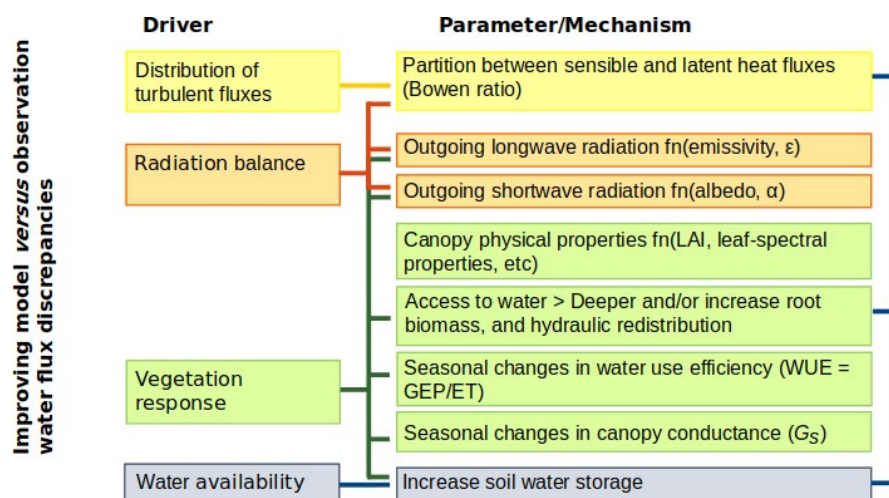

FIGURE 1 Parameters and mechanisms that govern ecosystem water fluxes (evapotranspiration) and their seasonality included in this study—water availability, vegetation response, radiation balance, and distribution of turbulent fluxes. Colored lines show which drivers interact with which parameters/mechanisms [Colour figure can be viewed at wileyonlinelibrary.com]

FIGURE 2 Locations of eddy covariance tower study sites in the Amazon Basin sensu stricto (Eva & Huber, 2005). Mean monthly net radiation (W m^{-2}) from the Clouds and the Earth's Radiant Energy System v4.0 (CERES; Kato et al., 2012) for the years 2003–2018 (NASA, 2019) [Colour figure can be viewed at wileyonlinelibrary.com]

Net radiation (W m^{-2})
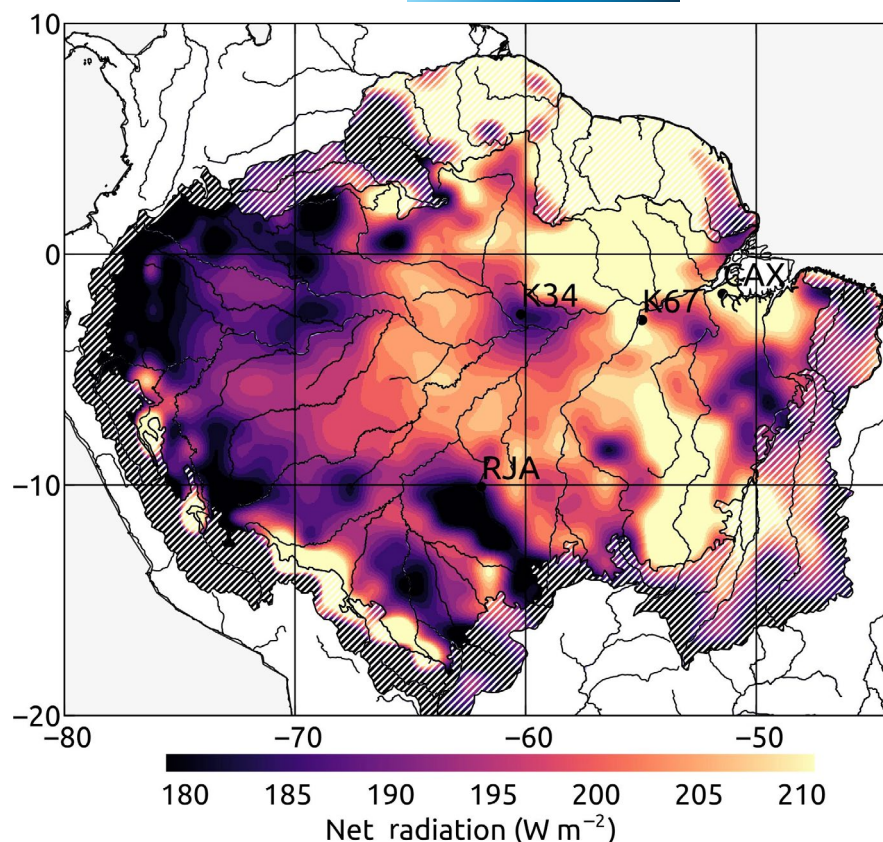
Ji-Paraná Reserva Jaru (RJA) forest, is located at the southern margins of the basin, at latitude 10°S. For a detailed site description, refer to previous works by da Rocha et al. (2009), Restrepo-Coupe et al. (2013, 2017), and Table S1.

2.2 | Eddy flux (EC), meteorological and biometric data

Sensible heat (H), water (ET) and carbon fluxes (F_c) were measured using the EC method (Baldocchi et al., 1988; Wofsy et al., 1993). Hourly average covariances were obtained from high frequency observations (20 Hz) of vertical wind velocity, virtual temperature (T_{son}; °C), and water (H_2O_{mix}; mmol mol^{-1}) and carbon dioxide (CO_2; ppm) mixing ratios measured with a 3D sonic anemometer (CSAT) and an infrared gas analyzer (LI6262; Burba, 2010; Foken et al., 2012). The LE was calculated as the product of water mass transfer (ET; mm day^{-1}) and latent heat of vaporization (λ; MJ kg^{-1}), where LE = ET λ. λ was calculated as a function of air temperature (Brutsaert, 1982).

Meteorological observations included: air temperature (T_{air}; °C), relative humidity (RH; %), precipitation (Precip; mm), wind speed (ws; m s^{-1}), turbulence measured as friction velocity (u_*; m s^{-1}), and the following radiation fluxes in W m^{-2}: incoming (SW_{down}) and outgoing shortwave (SW_{out}), and incoming (LW_{down}) and outgoing longwave (LW_{out}). Net radiation (R_n; W m^{-2}) was defined as the balance between incoming and outgoing fluxes (R_n = SW_{down} − SW_{out} + LW_{down} − LW_{out}). A four-dome net radiometer, CNR1 (Kipp & Zonen CM3

ISO-class, thermopile pyranometer, CG3 pyrgeometer, PT100 RTD) was used for the measurement of SW_{down}, SW_{out}, LW_{down}, and LW_{out} at all sites. The shortwave (SW) or solar radiation was defined as broadband radiation between 0.3 and 3 µm and the longwave (LW) as radiation with a spectral range from 3 to 300 µm. An independent R_n measurement from a single-component radiometer was available at K34 and K67.

Hourly data were subject to various quality control procedures: Values found to be outside ±3 standard deviations from the mean were removed for ws, RH, and T_{air}. Analogous and concurrent measurements were used to identify periods of instrument malfunction (e.g., T_{son} and T_{air}) recognized by observations outside two times the standard deviations from the linear relationship between the variables. Similar to processing carbon flux data, we removed LE fluxes measured during low turbulence conditions (given a site-specific u_* threshold, $u_{*thresh}$), thus the EC method's no-advection assumption does not apply (see Restrepo-Coupe et al. 2013; Table S1).

The energy balance was defined as R_n − Δ = LE + H + ΔSh + ΔSc + ΔSb, where ΔSh is the sensible heat storage on the canopy layer storage, ΔSc is the energy change due to photosynthetic activity, ΔSb is the biomass heat storage, and Δ is the imbalance (Figures S1 and S2). The Δ term includes measurement errors (e.g., differences between the footprint of the radiation sensor and the EC and loss of low frequency large-scale eddies) and unaccounted fluxes: ground heat flux (G) and changes in the LE flux stored on the air column below the EC system (ΔSle). At K34 where profile temperature

observations were not available, Δ included ΔSh and ΔSb, as well. ΔSh was calculated as the hourly change in temperature across the air column (eight, five, and four height levels at K67, RJA, and CAX, respectively) multiplied by air density and specific heat at constant pressure (Figure S3). ΔSc was defined as the product of gross ecosystem productivity (see Section 2.4) and the specific energy of conversion due to photosynthesis (1.088×10^4 J gCO$_2^{-1}$; Moderow et al., 2009). We calculated ΔSb as the product of canopy-specific heat capacity ($C_{veg} = 2958$ J kg^{-1} K^{-1}), live wet biomass (m_{veg}; kg m^{-2}) and the change in temperature at canopy level (T_{cpy}; K). See Supporting Information for m_{veg} values and T_{cpy} heights. To flag possible outliers, as part of our QA procedures, we used the slope of the regression (R_n vs. LE + H + ΔSh + ΔSc + ΔSb) assuming the observations outside two times the standard deviations from the linear relationship (see Figure S6).

We reviewed the seasonality of the energy balance residual as to improve the confidence in our analysis rather than determine LE-corrected values (i.e., we did not force energy balance closure). Note that we observed no statistically significant differences in the seasonal (monthly) energy balance closure (Figures S1 and S5). For an extensive review of the energy balance problem, the reader is invited to refer to the work of Foken (2008), subsequent studies (Mauder et al., 2018; Reed et al., 2018), and our Supporting Information.

At each EC site, meteorological drivers for the LSMs were generated from the standard suite of climatic variables available for periods between 1999 and 2006. We analyzed data for 2000–2005 for K34, 2002–2004 for K67, 2000–2002 for RJA, and 1999–2003 for CAX. Drivers included: LW$_{down}$, SW$_{down}$, T_{air}, ws, near-surface specific humidity (Q_{air}; g kg^{-1}), rainfall (Precip; mm month^{-1}), and surface atmospheric pressure (P_a; hPa; Figure 3). The CO_2 concentration (CO_{2air}; ppm) was fixed at 375 ppm, the average value during the period of measurements (de Goncalves et al., 2009). Observational data were filled using other nearby meteorological sites and/or the mean monthly diurnal cycle; however, only successive years with gaps no larger than two consecutive months were accepted. Although model drivers were gap-filled, regressions and other calculations presented in this manuscript were implemented using only non-filled flux observations and meteorological values. We sampled the EC data to match the timing of the model drivers and output.

Biogeochemical fluxes can be sensitive to canopy structure and function. For our analysis we used 16-day values of leaf area index (LAI), net primary productivity (NPP) allocated to leaves (NPP$_{leaf}$; gC m^{-2} day^{-1}), wood (NPP$_{wood}$; gC m^{-2} day^{-1}), and litterfall (NPP$_{litter}$; gC m^{-2} day^{-1}). Litterfall data were available for all forests and included recently published values by Freire et al. (2020) for RJA. We used previously published LAI values—see Table S1 for references,
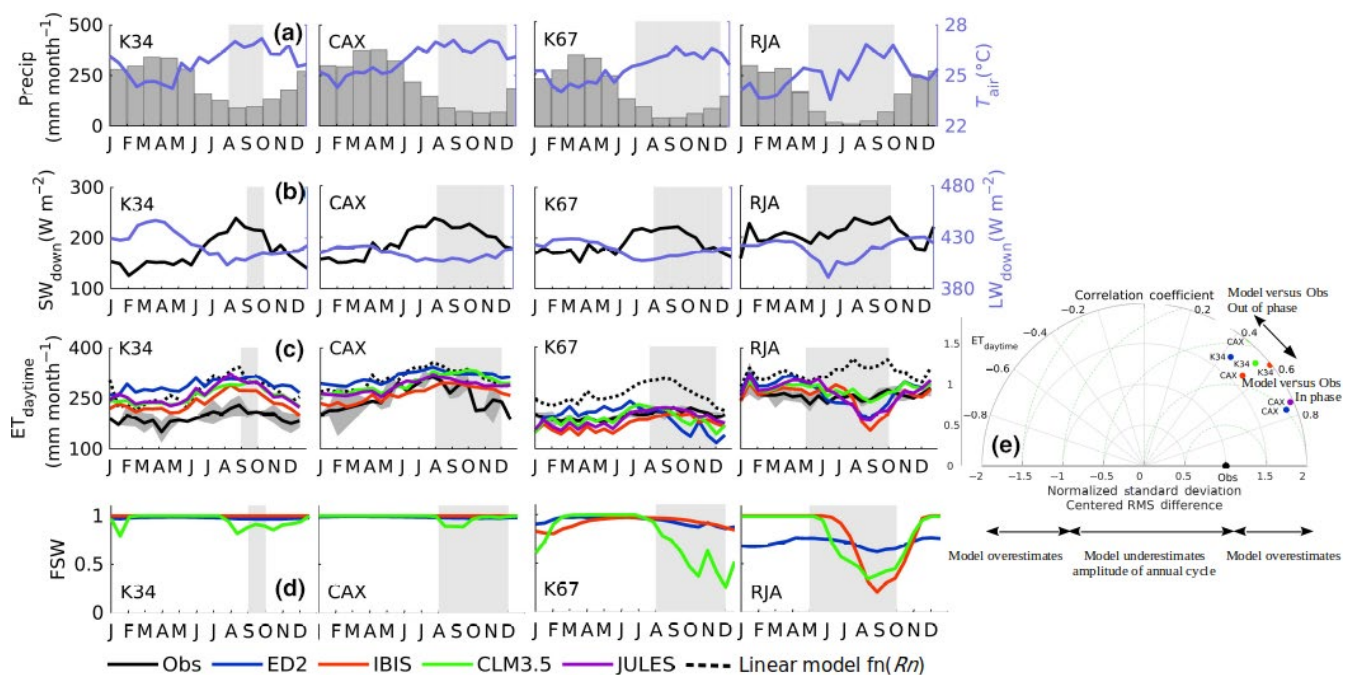

FIGURE 3 Annual cycle 16-day average observed climatic drivers (a) precipitation (Precip; mm month^{-1}; gray bars), air temperature (T_{air}; °C; blue line left y-axis) and (b) incoming shortwave (SW$_{down}$; W m^{-2}; black line right y-axis) and longwave radiation (LW$_{down}$; W m^{-2}; blue line left y-axis). (c) Modeled and observed daytime evapotranspiration (ET$_{day}$, mm month^{-1}); dashed line corresponds to the reference evapotranspiration (model ET driven only by meteorology). (d) Model ecosystem scale of model soil moisture "stress" (FSW, where 1 = no stress). From left to right study sites (from wettest to driest) near Manaus (K34), Caxiuanã (CAX), Santarém (K67), and Reserva Jaru southern (RJA) forests. Gray shaded area is dry season as defined using satellite-derived measures of precipitation (TRMM: 1998–2018). (e) Right-hand plots correspond to Taylor diagrams for a statistical summary of model (color coded) fluxes compared to observations of seasonal fluxes (16-day). Missing sites indicate that the model overestimates the seasonality of observations; the ratio between modeled (σ_m) and observed standard deviations (σ) is >2. Simulations from ED2 (blue), IBIS (red), CLM3.5 (green), and JULES (purple) [Colour figure can be viewed at wileyonlinelibrary.com]

values, and methods. For a description of biometric sampling methods, see the original works of Metcalfe et al. (2007), Brando et al. (2010), Rice et al. (2004), and Fisher et al. (2007), and for calculations and a description of the *NPP* seasonal values, see Restrepo-Coupe et al. (2017).

2.3 | Surface emissivity (ε_s), Bowen ratio, outgoing longwave radiation (LW_{out}), and other calculations

We used observations of the longwave radiation balance (LW_{down} and LW_{out}) as per the integral of the Planck radiation function, the Stefan–Boltzmann equation, to obtain the measure of the surface's ability to emit energy by radiation, the Earth's surface spectral emissivity (ε_s):

$$LW_{out} = \varepsilon_s \sigma_{SB} T_{skin}^4 + (1 - \varepsilon_s) LW_{down}, \qquad (1)$$

where σ_{SB} is 5.6704×10^{-8} W m^{-2} K^{-4} the Stefan–Boltzmann constant, T_{skin} is the skin temperature (K), and ε_a is the effective emissivity of the atmosphere (Jin & Liang, 2006). The equation included the reflected fraction of LW_{down} the second term (($1 - \varepsilon_s$) LW_{down}), following Kirchhoff's law, which assumes that absorptivity and emissivity are the same for each spectral band (Liou, 2002). We used canopy level temperature measurements (lagged as to reach a maximum four hours after peak T_{air}) as a proxy for T_{skin} (Moderow et al., 2009; see Supporting Information section 4). No contact thermometry was installed at any of the study sites. We solved for ε_s:

$$\varepsilon_s = \frac{LW_{out} - LW_{down}}{\sigma_{SB} T_{skin}^4 - LW_{down}}. \qquad (2)$$

The derivation of ε_s is a simplification of a complex process: We did not account for the vertical variations of T_{air}, and we neglected the re-emission of LW radiation by water vapor. Nonetheless, we are measuring LW_{down} and LW_{out} at the four forests and we see this calculation as an improvement over the assumed emissivity values used by some LSMs. Similarly, to identify possible bias on model LW_{out} calculations, we solved Equation (2) for T_{skin} assuming ε_s values of 0.99 (see Supporting Information section 4).

Here we include 1-km grid MOD11A2.v6 (Wan et al., 2015), the land surface temperature (LST) product to scale and compare T_{air} measurements to satellite-derived LST used by some models on their emissivity calculations (Figure S8).

To describe the forest optical brightness, we calculated the daytime albedo (top of the atmosphere radiation, TOA >200 W m^{-2}) as the unitless ratio of outgoing to incoming solar radiation (α = SW$_{out}$/SW$_{down}$). We computed the TOA following Goudriaan (1986) and set a threshold of TOA and SW$_{down}$ >200 W m^{-2} to constrain daytime observations. To characterize the heat transfer and the partition between water and sensible heat fluxes, we used the Bowen ratio calculated as the fraction of *H* to LE (Bowen = *H*/LE).

The Bowen ratio is used by some models as a driver in stomatal conductance and photosynthesis calculations (Berry et al., 2013; Sellers, 1985).

2.4 | Vegetation contributions to ET

To quantify the vegetation response to meteorology, we evaluated the seasonal differences between observed ET and the reference ET (ET$_{ref}$; also known as potential ET). The ET$_{ref}$ is solely driven by atmospheric demand and climatic parameters and is independent of the vegetation water use and soil factors. The ET$_{ref}$ was calculated following the FAO Penman–Monteith method as:

$$ET_{ref} = \frac{\delta}{\delta + \gamma} Rn, \qquad (3)$$

where γ is the psychrometric coefficient ($C_p P_a 10^3/0.622 \lambda$; kPa K^{-1}), δ is the slope of vapor pressure curve ($\delta = 4098 e_{sat}/T_{air}^{-2}$; kPa K^{-1}), and C_p is the specific heat of air at constant pressure (J kg^{-1} K^{-1}).

We calculated the ecosystem water use efficiency (WUE) as the ratio between daytime photosynthetic activity (TOA >200 W m^{-2}) measured as the gross primary productivity (GPP$_{day\&dry}$; gC m^{-2} day^{-1}) to ET$_{day\&dry}$ over a 16-day period (WUE = GPP$_{day\&dry}$/ET$_{day\&dry}$; gC mm^{-1}). The ET$_{day\&dry}$ (mm day^{-1}) was measured excluding observations during and 12 h after precipitation, and using only daytime data, and was assumed to be the ET dominated by transpiration (*T*) fluxes rather than by direct evaporation (*E*) from interception (e.g., after rain) and from condensation (e.g., dawn measurements). Similarly, the TOA threshold removed all early morning–late afternoon values from the WUE calculations, thus small ET values translated into abnormally high efficiencies without physical merit. Here, we use the term gross primary productivity (GPP) interchangeably with gross ecosystem productivity (GEP; gC m^{-2} day^{-1}) and negative gross ecosystem exchange (GEE; gC m^{-2} day^{-1}), where GPP ~ GEP = – GEE (Stoy et al., 2006). The GEE was estimated from the measured daytime net ecosystem exchange (NEE; gC m^{-2} day^{-1}) by subtracting estimates of ecosystem respiration (R_{eco}; gC m^{-2} day^{-1}), which in turn were derived from nighttime NEE (GEE = –NEE + R_{eco}). The NEE was calculated as the sum of the fluxes measured at the top of the tower and the CO_2 storage flux (NEE = F_c + S_{CO2}) and filtered for low turbulence periods (site-specific $u_{*thresh}$). R_{eco} was calculated as the average within a centered 5-day wide moving window, assuming at least eight valid hours of nighttime NEE (we expanded the window up to 30 days until sufficient valid data were included). The selected R_{eco} moving window accounts for sensitivity to seasonally varying soil moisture. Daytime R_{eco} was assumed to be equal to nighttime R_{eco}. See Supporting Information and Restrepo-Coupe et al. (2013, 2017) for uncertainty analysis and additional methods.

To better understand the contribution of vegetation to LE and consequently to the partition of turbulent heat fluxes (Figure 1), we calculated the canopy stomatal resistance to water vapor (*rsV*; s m^{-1}) and the corresponding canopy conductance (G_s; mmol m^{-2} s^{-1})

following the flux-gradient method as described by Wehr and Saleska (2015, 2021; see Supporting Information section 6 for calculations and sensitivity analysis).

2.5 | Land surface models

We present output from four process-based LSMs that were part of the "Interactions Between Climate, Forests, and Land Use in the Amazon Basin: Modeling and Mitigating Large-Scale Savannization" project (Powell et al., 2013; Restrepo-Coupe et al., 2017). We used the Community Land Model-Dynamic Global Vegetation Model version 3.5 (CLM3.5; Gotangco Castillo et al., 2012; Oleson et al., 2008; Stockli et al., 2008), the Ecosystem Demography model version 2 (ED2; Longo et al., 2018; Longo, Knox, Medvigy, et al., 2019; Medvigy et al., 2009), the Integrated Biosphere Simulator (IBIS; Foley et al., 1996; Kucharik et al., 2000), and the Joint UK Land Environment Simulator (JULES v.2.1; Best et al., 2011; Clark et al., 2011). The LSM energy and water cycle dynamics, including how radiation and conductance were calculated by models, are presented in Table S2.

Models compute R_n as the sum of LW_{down} and SW_{down} (forcing drivers) minus the outgoing energy flux, the LW_{out} and SW_{out} calculated using parameters assigned to a plant functional type (PFT) and/or via different canopy radiation transfer models and equations (e.g., the two-stream model and the Beer–Lambert law; Fisher et al., 2018). Later, R_n is partitioned into LE and H. This partition is determined by atmospheric demand and the amount of water available for evaporation and transpiration (if the water supply is exhausted, energy will ultimately be spent exclusively on H). If water is available, LE will be driven by temperature, wind velocity, available radiant energy, and will be modulated by G_s and aerodynamic conductance (G_i; Figure 1). The G_s, representing the exchange of CO_2 and H_2O between multiple canopy leaves and the atmosphere, is controlled by meteorological and edaphic conditions given the ecosystem's structure, and by plant trait expressions that determine the photosynthetic capacity (e.g., quality and quantity of leaves and stomatal behavior). Therefore, G_s links the energy, carbon, and water cycles, and constitutes a key vegetation status descriptor for LSMs.

LSMs calculated the downregulation factor for stomatal conductance due to soil water stress (FSW; also known as the β term) following Oleson et al. (2008; CLM3.5) and Castanho et al. (2016; ED2, IBIS, and JULES). The FSW factor ranges from 0 (maximum stress) to 1 (no stress).

Model diagnostic variables complied with radiation energy and water conservation equations (Equation 4 and 5). The energy balance residual was always smaller than 1 W m^{-2}:

$$SW_{down} - SW_{out} + LW_{down} - LW_{out} - H - LE - G = \Delta S_b + \Delta S_h, \quad (4)$$

And the water balance residual was less than 1×10^{-6} kg m^{-2} s^{-1}, defined by:

$$Prec - ET - R - GW + F = \left(\Delta_{intercept} + \Delta_{srfstor} + \Delta_{soilmoist} \right) / dt, \quad (5)$$

where R is surface runoff, GW is subsurface runoff, F is recharge from rivers, and $\Delta_{intercept}$, $\Delta_{srfstor}$, and $\Delta_{soilmoist}$ are changes in interception, surface storage, and soil moisture, respectively (all values in units of kg m^{-2} s^{-1}).

2.6 | Calculating seasonality and comparing models to observations

For each hour on the 16-day period we used all available measurements (minimum four observations per hour; Figure S7). We calculated the mean of the average daily cycle (minimum 22/24 h of the cycle was required for calculation of seasonal mean). This method avoids assigning less weight to those periods where we have fewer measurements. For example, at K34 precipitation was common in the late afternoon; therefore, LE, H, and other measurements that depend on the sonic anemometer were unavailable during rainfall events (Figure S9). Seasonal WUE (GEP$_{day\&dry}$/ET$_{day\&dry}$) and ET/ET$_{ref}$ were calculated using 16-day ratios. The average annual cycle was calculated from all available 16-day periods when at least two measurements were available (2 years of data for each period).

Models were compared to observations based on the timing and amplitude metrics of their annual cycle. Correlation coefficient (r), root-mean-square difference of model-observations (RMSE), and the ratio of their variances were determined for the 16-day multiple years' time series and the difference in amplitude and timing of the seasonal cycle were summarized using the unitless normalized standard deviation calculated as the ratio between modeled (σ_m) and observed (σ) standard deviation via Taylor diagrams (Taylor, 2001; see Figure 3e for its interpretation). Sites missing from figures indicate that the model overestimated the seasonality of observations and σ was >2.

We used Type II linear regressions between fluxes, parameters, and variables to understand and quantify the relationships between flux drivers and meteorological variables (e.g., H vs. R_n) and between ecosystem characteristics and processes (e.g., LAI vs. albedo), thus acknowledging both variables carried some degree of uncertainty. To describe the statistical significance of regressions, we calculated p-values and the coefficient of determination (r^2), and the Akaike's information criterion, among other descriptors. We compared the resulting linear models to simulations (benchmark) to identify key flux drivers and determine when and how LSMs can be underutilizing the available variable information (Abramowitz, 2005; Best et al., 2015).

3 | RESULTS

3.1 | Seasonal meteorology and ET

All sites showed contrasting degrees of seasonality in terms of rain, temperature, insolation, and/or day length, including differences in the amplitude of the radiation and precipitation annual cycles and

the timing metrics that define the start, end, peak, and dry-season length (Figure 3). Mean annual precipitation at RJA and K67 was close to 2000 mm compared to 2500 mm at CAX and K34. The dry season varied in length and strength from 1 month long at K34 to 5 months at K67 and RJA (Figure 3). Although the dry season at K34 only lasted for 1 month (August), there was a period from July to October when the precipitation was lower than the annual mean and when we observed above average incoming radiation values (similar seasonality to K67 and CAX). The number and intensity of precipitation events was different: (1) CAX with frequent-low intensity rainfall (≥250 events month^{-1} of <0.5 mm h^{-1}), (2) strong seasonal changes at RJA (dry season with few lower than 0.5 mm h^{-1} intensity events and wet season with ~50 events higher than 2.5 mm h^{-1}), and (3) K67 and K34 close to aseasonal intensities (2.5 mm h^{-1}); however, there were fewer events at K67 (≤50 events month^{-1}) compared to K34 (≤100 events month^{-1}; Figure S9).

The observed annual cycle of ET showed three different patterns across forests: (1) maximum water vapor flux at the beginning of the dry season declining as the season progressed at the two wettest locations (K34 and CAX); (2) a well-defined ET cycle, with a middle of the dry-season peak at K67; and (3) an aseasonal LE flux at the southern forest of RJA (Figures 3c and 4a). Modeled ET showed seasonal synchronicity with observations at the two wettest sites (K34 and CAX); however, LSMs overestimated the dry-season flux by 150–20 mm month^{-1} (Figure 3c). At K67 and RJA,

models exaggerated the amplitude of the water flux seasonal cycle by 180–20 mm month^{-1}. At these drier locations, LSMs predicted reductions in dry-season ET that were generally driven by the available soil moisture, as demonstrated by the statistically significant relationship between flux and the plant-available water model diagnostic FSW ($p < 0.01$ r^2 from 0.1 (IBIS) to 0.7 (ED2) at K67 and 0.3 (ED2) to 0.7 (CLM3.5) at RJA; Figure 3d; Figure S10). By contrast, observations showed available energy driving ET at all sites (Table S3). The slope of the regression between seasonal LE versus R_n (type II, zero intercept) was ~0.6 (Figure S11; $r^2 = 0.7$ at CAX, 0.8 at K34, 0.5 at K67, and 0.1 at RJA). Seasonal T_{air} and LE showed a significant positive correlation ($r^2 = 0.42$, $p < 0.01$) at only one site, K67 (Table S3). The ET_{day} was close to constant (7.7 mm day^{-1}) at the southern forest of RJA. RJA was the only forest where we observed no significant correlation between R_n and ET ($r^2 < 0.1$, $p = 0.9$); however, the linear model had a low RMSE value (7.78 W m^{-2}). Moreover, all site regressions between R_{nday} and LE_{day} showed RJA observations following the general trend (Figure 8).

3.2 | Partition of net radiation into turbulent fluxes

At the equatorial Amazon forests (K34, CAX, and K67), the 16-day cycle of H showed a maximum at the beginning and a minimum at the end of the dry season (Figure 4b). By contrast, H was close to
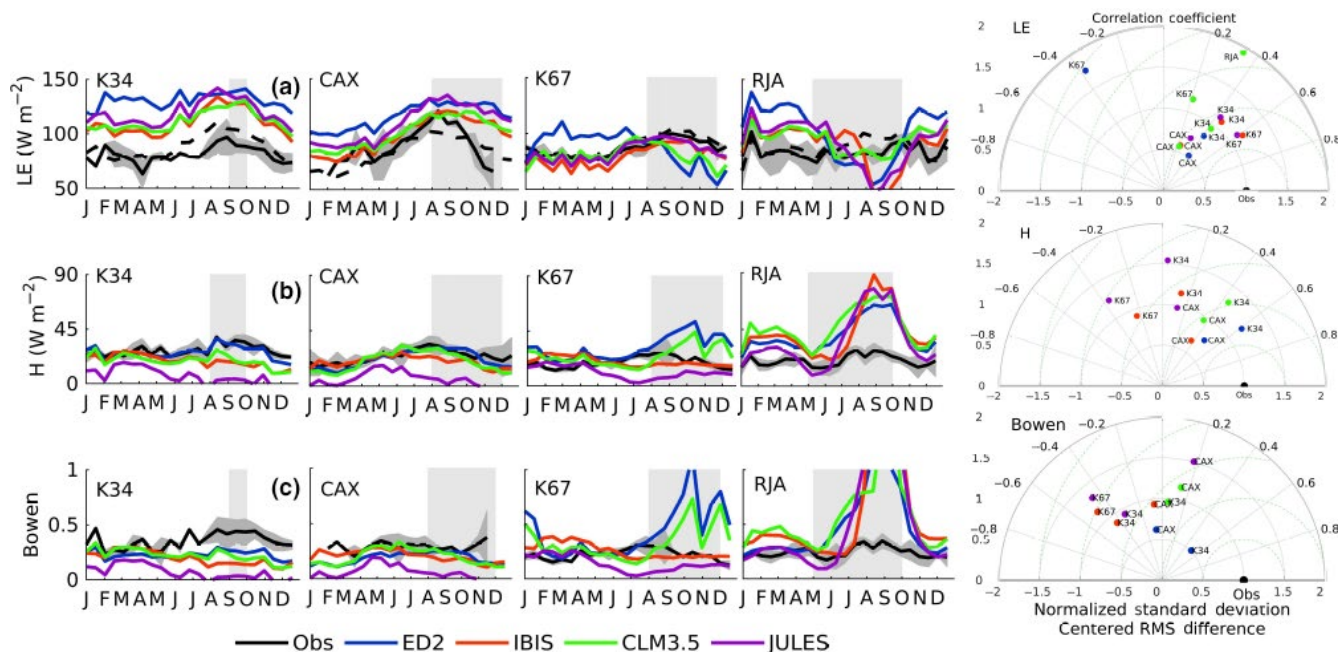

FIGURE 4 Annual cycle 16-day average of (a) latent heat flux (LE; W m^{-2})—energy equivalent of evapotranspiration (ET; mm day^{-1}), and model results from a linear regression between LE and R_n (dashed black line). (b) Sensible heat flux (H; W m^{-2}) and (c) unitless Bowen ratio (Bowen = H/LE). From left to right study sites (from wettest to driest) near Manaus (K34), Caxiuanã (CAX), Santarém (K67), and Reserva Jaru southern (RJA) forests. Observations (black line) and corresponding standard deviations (σ) (dark gray shaded area) and simulations (color lines) from ED2 (blue), IBIS (red), CLM3.5 (green), and JULES (purple). Light gray shaded area is dry season as defined using satellite-derived measures of precipitation (TRMM: 1998–2018). Right-hand plots correspond to Taylor diagrams for a statistical summary of model (color coded) fluxes compared to observations of seasonal fluxes (16-day). Missing sites indicate that the model overestimates the seasonality of observations; the ratio between modeled standard deviation (σ_m) and σ is >2 [Colour figure can be viewed at wileyonlinelibrary.com]

aseasonal at RJA (a slight increase by the middle of the dry period). Models were able to capture the seasonal cycle of H at CAX; however, the dry-season H was underestimated by most of the LSMs at K34. LSMs overestimated LE and were out of phase with observations at K67 and RJA (Figure 4b). At K34 and RJA, the relationship between observed H and LE was weak ($r^2 < 0.2$, $p < 0.01$) and significant at CAX and K67 ($r^2 = 0.6$, $p < 0.01$; Figure S11). At RJA and CAX, measurements of R_n explained 50% of the H seasonal variability. Moreover, H was significantly correlated with R_n, the slope (zero intercept) varying from 0.12 at K67, 0.15 at CAX and RJA, to 0.22 at K34 ($r^2 \sim 0.4$, $p < 0.01$; Figure S11).

Observations showed that Bowen ratio values were nearly constant at ~0.32 for K34 (highest) and at ~0.21 for RJA and K67 (lowest among forests). We found that the Bowen ratio for the four LSMs was lower than the observed value at the two wettest locations (K34 and CAX) and above measurements at the two driest forests (K67 and RJA). Simulations showed a strong increase in Bowen ratio during the dry season at K67 (IBIS and ED2) and at RJA (all models; Figure 4c).

Hourly and seasonal observations showed a good seasonal energy balance closure (slope LE + H vs. R_n) ranging from 90% (CAX), 88% (K67 and K34) to 83% (RJA; Figures S1 and S2). By comparison, FLUXNET sites have an average imbalance of ~20% (Wilson et al., 2002). Where profile temperature data were available, the introduction of canopy and biomass heat storage improved the overall hourly

balance, especially the energy closure at dawn and dusk (see Figure S3). Δ showed a statistically significant correlation to R_n ($\Delta \sim 0.1R_n$, $r^2 > 0.8$, $p < 0.01$) and no correlation with turbulence, T_{air}, or rainfall (Figures S3 and S4). Therefore, we had no indication of lost fluxes due to advection (low u_*) or errors associated with turbulence bursts (high u_*). At CAX, frequent rainfall events made EC measurements challenging, and extensive periods of data needed to be removed (causing gaps in many regressions and figures). Rainfall events at CAX were less intense; however, they were more frequent than at any other site (see Figure S9).

3.3 | Radiation balance: Outgoing longwave (LW_{out}) and reflected shortwave (SW_{out}) radiation

The SW_{out} is determined by the surface reflectance (e.g., we see low SW_{out} values in dark bodies, and high values in bright bodies) and its relation to SW_{down} is measured as albedo (α; Figure 5). Seasonality of α showed modest increases as the dry season progressed at all sites and was in-phase with the radiation seasonal cycle (Figure S15). Peak α values (when forest was at its brightest) were observed by the middle of the dry season at the equatorial Amazon sites (CAX, K34, and K67) and at the end of the dry period at RJA (Figure 6a). The average α was 0.12 at RJA, K34, and K67, and 0.09 at CAX. Negative regressions between precipitation
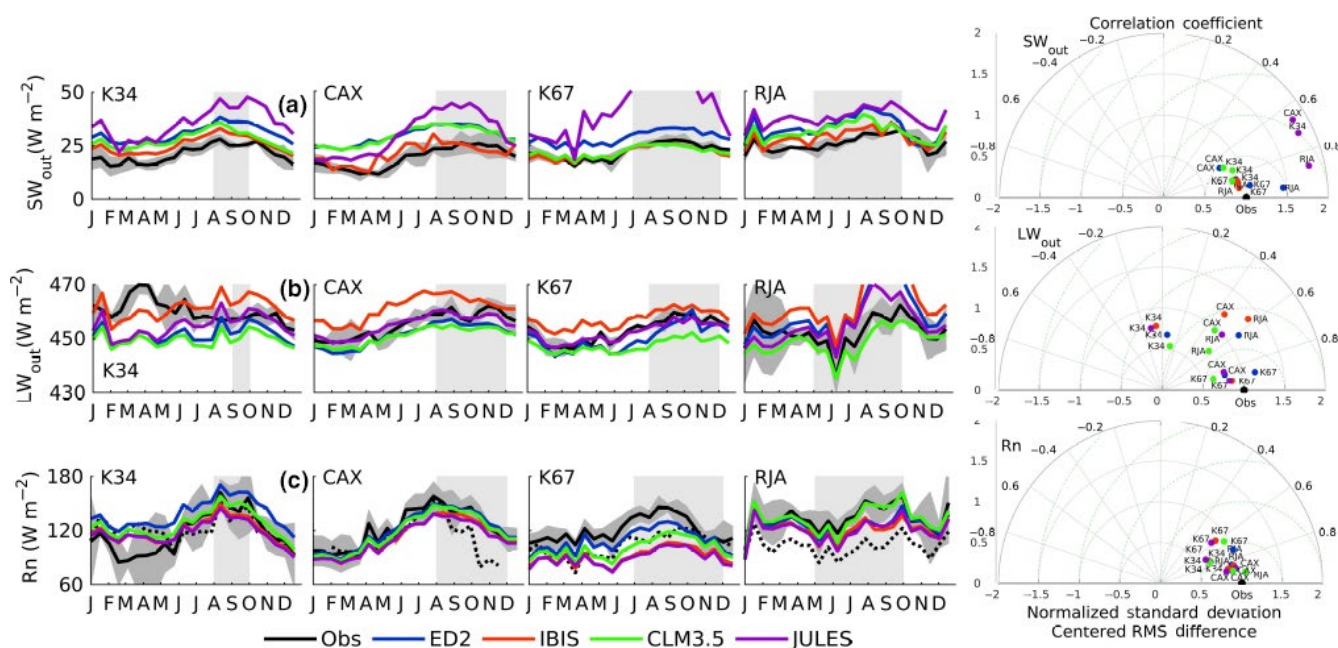

FIGURE 5 Annual cycle 16-day average of (a) outgoing shortwave radiation (SW_{out}; W m^{-2}), (b) outgoing longwave radiation (LW_{out}; W m^{-2}), and (c) net radiation (Rn; W m^{-2}; black continuous line), and the sum of turbulent fluxes, sensible plus latent heat flux (H + LE; W m^{-2}; black dotted line). From left to right study sites (from wettest to driest) near Manaus (K34), Caxiuanã (CAX), Santarém (K67), and Reserva Jaru southern (RJA) forests. Observations (black line) and corresponding standard deviations (σ) (dark gray shaded area) and simulations (color lines) from ED2 (blue), IBIS (red), CLM3.5 (green), and JULES (purple). Light gray shaded area is dry season as defined using satellite-derived measures of precipitation (TRMM: 1998–2018). Right-hand plots correspond to Taylor diagrams for a statistical summary of model (color coded) fluxes compared to observations of seasonal fluxes (16-day). Missing sites indicate that the model overestimates the seasonality of observations; the ratio between modeled standard deviation (σ_m) and σ is >2 [Colour figure can be viewed at wileyonlinelibrary.com]
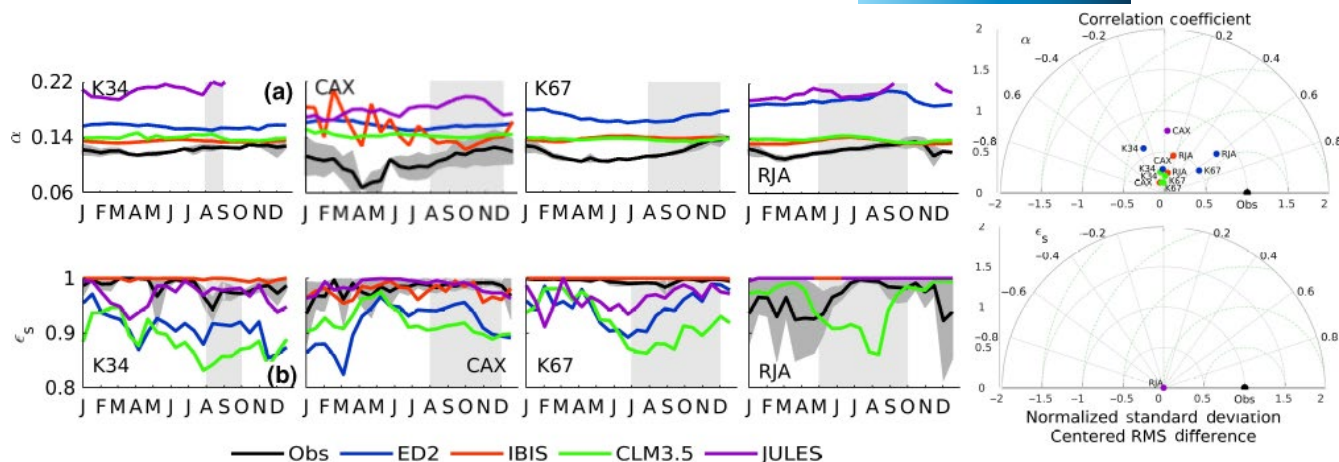
FIGURE 6 Annual cycle 16-day average of (a) albedo—the ratio of outgoing to incoming shortwave radiation ($\alpha = SW_{out}/SW_{down}$), and (b) surface emissivity (ε_s). From left to right study sites (from wettest to driest) near Manaus (K34), Caxiuanã (CAX), Santarém (K67), and Reserva Jaru southern (RJA) forests. Observations (black line) and corresponding standard deviations (σ) (dark gray shaded area) and simulations (color lines) from ED2 (blue), IBIS (red), CLM3.5 (green), and JULES (purple). Light gray shaded area is dry season as defined using satellite-derived measures of precipitation (TRMM: 1998–2018). Right-hand plots correspond to Taylor diagrams for a statistical summary of model (color coded) fluxes compared to observations of seasonal fluxes (16-day). Missing sites indicate that the model overestimates the seasonality of observations; the ratio between modeled standard deviation (σ_m) and σ is >2 [Colour figure can be viewed at wileyonlinelibrary.com]

and α (the forest was darkest at the peak of the wet season) were statistically significant at all forests ($p < 0.01$ with r^2 values up to 0.4 at K67 and K34; Figure S13). The forest characteristics showed some degree of correlation: (1) low LAI to high α (negative slope) at CAX; and (2) high NPP_{leaf} to high canopy brightness (positive slope) at K67, RJA, and K34 (Figure S14). However, at all sites, the timing of maximum α did correlate with peak leaf-flush greenness index phenocam observations (e.g., Lopes et al., 2016). Models overestimated α annual mean across sites and underestimated the amplitude of the α seasonal cycle.

Observations showed mean monthly values of SW_{out} close to 20 W m^{-2} at most forests (Figure 5a). The models captured the seasonal cycle of SW_{out} at all sites except RJA. The SW_{out} was significantly correlated with SW_{down} ($r^2 = 0.9$ at K34 and RJA, 0.7 at K67 and $r^2 = 0.5$ at CAX; $p < 0.01$), with the slope of their linear relationship increasing from wet to dry forests, such as 0.12 at K34 and CAX, 0.13 at K67 and 0.14 at RJA (Figure S15). Seasonal LW_{out} was significantly correlated with LW_{down}; however, R^2 values were low ($r^2 = 0.34$ at K34, 0.5 at K67 and $r^2 = 0.2$ at CAX and RJA, $p < 0.01$) with a positive slope at K34 and RJA and a negative regression (LW_{down} increased faster than LW_{out} and surface-canopy temperature warming at a lower rate than the air) at CAX and K67 (Figure S17). At K67, CAX, and RJA, models captured the amplitude of the seasonal LW_{out} cycle; however, at K34, the LW_{out} of all model simulations was out of phase with observations (Figure 5b).

The amplitude of the annual surface emissivity (ε_s) cycle representing the ability of the surface to emit longwave radiation showed high dry-season values at RJA and CAX (Figure 6b). By contrast at CAX, observations showed low wet-season ε_s values. At K34 and K67, observed ε_s were higher than 0.98 and close to 0.95 at RJA. We found statistically significant correlations

(– <0.01, r^2 range 0.3–0.8) between ε_s and rainfall (positive) and T_{air} (negative) at K34 and vice versa at CAX—no significant correlation was observed at K67 and RJA (Figure S13). LSMs generally did not capture the magnitude or seasonality of ε_s, and no LSM aligned with observations across all sites (Figure 6b). Assuming constant ε_s values of ~0.99 in agreement with satellite measurements (Figure S8) showed models either overestimated T_{skin} (~1 to 5°C) or underestimated ε_s (Figure S12).

3.4 | Ecosystem characteristics and contributions to water and energy flux seasonality

The ratio between observed ET and ET_{ref} can be used to identify the periods when ET does not show any signs of water-supply limitation and the flux is mostly driven by atmospheric demand and solar radiation (Figure 3c; Figure S19). Only during the wettest months at K34 we observed ET equivalent to ET_{ref} (ET/ETref ~ 100%) and ~70% during the driest period (Figure 7a). In general, the slope of the regression between ET and ET_{ref} varied from 0.66 (RJA) to 0.74 (K67 and K34), with statistically significant differences between wet and dry-season values only seen at RJA and K34 (Figure S19).

The vegetation control over ET, here represented by G_s, showed different degrees of seasonality and trends across forests (Figure 7b); nevertheless, minimum values were observed at various times during the dry season at all sites: (1) At CAX, the dry-season G_s was close to 0.4 mmol m^{-2} s^{-1} and up to 1.4 mmol m^{-2} s^{-1}—the highest G_s values were observed at this site; (2) at K34 and K67, the G_s gradually decreased from the transition wet-to-dry period to reach minimum values at the onset of
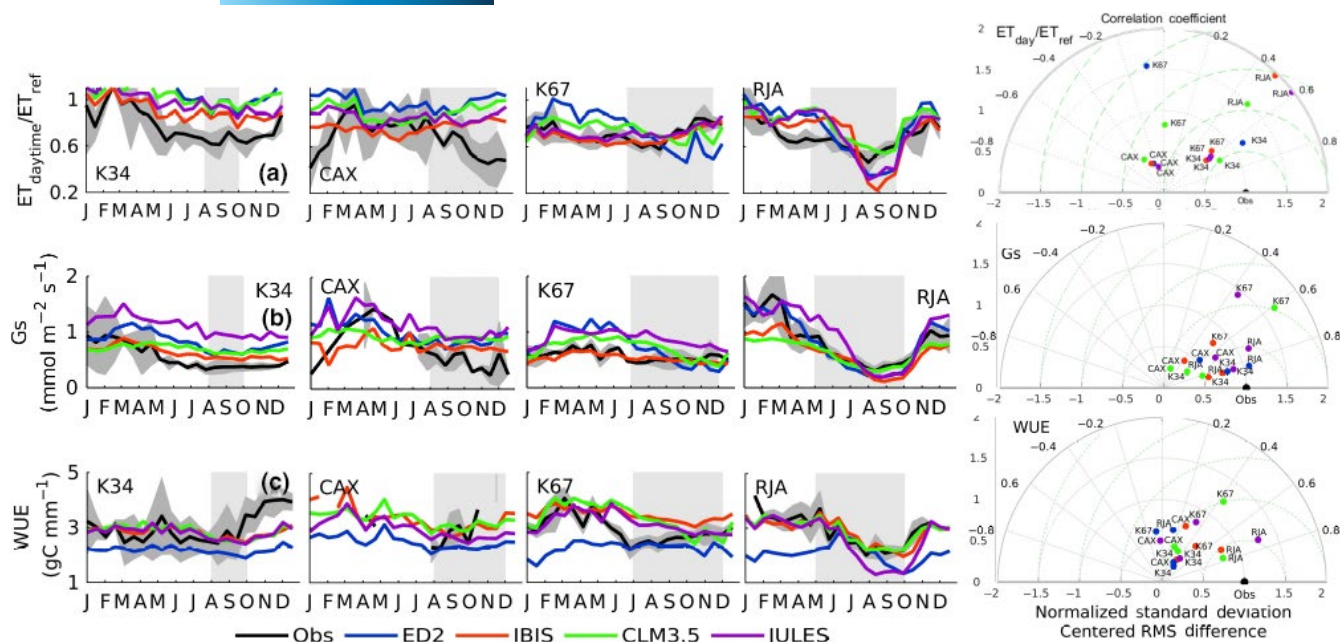
FIGURE 7 Annual cycle 16-day average of (a) ratio between the observed and reference evapotranspiration (ET/ET$_{ref}$), (b) canopy stomatal conductance (G_s; mmol m^{-2} s^{-1}), and (c) daytime water use efficiency where ET and GEP were sampled during dry conditions (no rain in prior 12 h) assuming transpiration drives water fluxes (WUE = GEP$_{dry\&dry}$/ET$_{dry\&dry}$; gC mm^{-1}). From left to right study sites (from wettest to driest) near Manaus (K34), Caxiuanã (CAX), Santarém (K67), and Reserva Jaru southern (RJA) forests. Observations (black line) and corresponding standard deviations (σ) (dark gray shaded area) and simulations (color lines) from ED2 (blue), IBIS (red), CLM3.5 (green), and JULES (purple). Light gray shaded area is dry season as defined using satellite-derived measures of precipitation (TRMM: 1998–2018). Right-hand plots correspond to Taylor diagrams for a statistical summary of model (color coded) fluxes compared to observations of seasonal fluxes (16-day). Missing sites indicate that the model overestimates the seasonality of observations; the ratio between modeled standard deviation (σ_m) and σ is >2 [Colour figure can be viewed at wileyonlinelibrary.com]
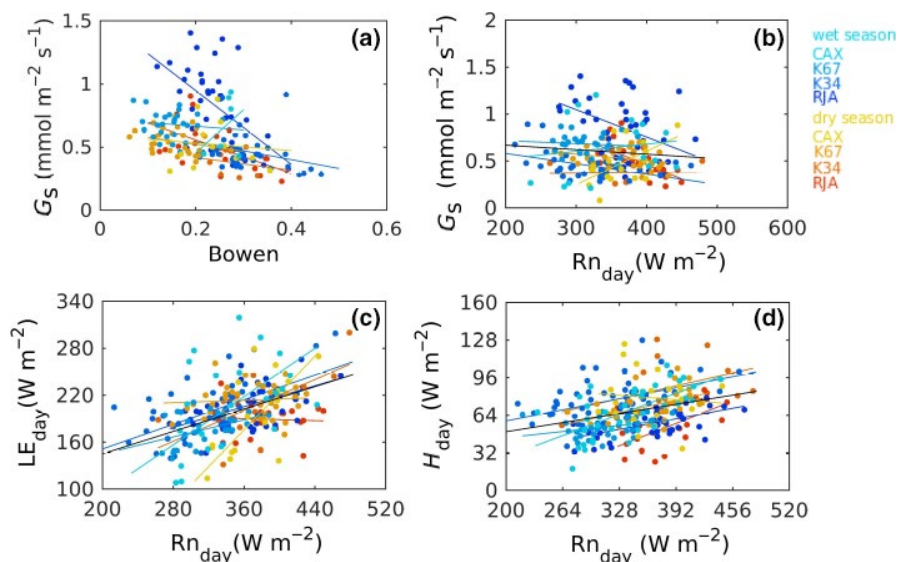

FIGURE 8 Relationships between seasonal 16-day average values of (a) canopy stomatal conductance (G_s; mm s^{-1}) and the ratio between sensible (H; W m^{-2}) and latent heat flux (LE; W m^{-2}), the unitless Bowen ratio (Bowen = H/LE); (b) G_s and daytime net radiation (R_{nday}; W m^{-2}); (c) daytime LE (LE$_{day}$; W m^{-2}) and R_{nday}; and (d) daytime H (H$_{day}$; W m^{-2}) and R_{nday}. Panels may include a linear regression for all available data (black line) and single regressions fitted for each site and seasons (color lines): Manaus (K34), Caxiuanã (CAX), Santarém (K67), and Reserva Jaru southern (RJA) forests if statistically significant. Seasons classified using satellite precipitation TRMM values (1996–2018), dry (rainfall <100 mm month^{-1}), and wet period (>100 mm month^{-1}) [Colour figure can be viewed at wileyonlinelibrary.com]

the rainy season. (3) RJA experienced a reduction in G_s mid wet season to mid dry season (an all site minima of 3 mmol m^{-2} s^{-1}). Models were able to capture G_s at most forests; however, they

underestimated the amplitude of the annual cycle at K34 and CAX (Figure 7b). The trade-off between losing water through transpiration and gaining carbon showed different patterns

across sites, suggesting leaf-level adaptations and ecosystem-level variation. For example, seasonal G_s showed a negative relationship to incoming radiation at K34, RJA, and during the dry season of K67 ($r^2 < 0.3$, $p < 0.01$). By contrast, higher SW_{down} correlated with high G_s at the very seasonal forest of CAX (where we observed the highest wet period rainfall values among the four forests) and during the wet season at K67 (Figure 8b; Figure S20). In general, G_s was positively related to precipitation (Figure S21).

The ratio between ecosystem carbon uptake and transpiration-dominated ET, here presented as WUE was correlated with G_s at CAX (negative, $r^2 = 0.25$, $p < 0.01$) and RJA (positive, $r^2 = 0.48$, $p < 0.01$; Figure S22). A significant regression was observed at K67 only if G_s was lagged by 2 months (minimum WUE preceded minimum G_s; Figure 7b). The WUE changes were non-significantly correlated to G_s at K34. Minimum WUE values were observed at the beginning of the dry season at equatorial sites (CAX, K34, and K67) and at the end of the dry period at RJA. The largest values of WUE, indicative of the highest photosynthetic rate per water use, were observed at different times for different sites when precipitation was >100 mm month^{-1} (start of at K34 and K67 and end of the wet season at RJA all at ~2.6 gC mm^{-1}; Figure 7c). Most models were able to correctly estimate seasonal values of WUE and G_s, some overestimating G_s values at K34 and WUE at K67.

We used the Bowen ratio to describe the dominant type of heat transfer across the forests—where LE clearly dominated the turbulent flux ($H < 0.2$ LE). The relationship between Bowen ratio and G_s showed that at relatively high Bowen values >0.3, the G_s reached a minimum of ~0.35 mmol m^{-2} s^{-1} (no further reductions were observed; Figure 8a).

4 | DISCUSSION

This study identified three main tropical forest properties (relationships among fluxes and between fluxes and vegetation characteristics) that if understood and implemented in LSM equations and/or benchmarking exercises could reduce the differences between observations and model estimates of seasonal ET, R_n, and H exchange: (1) Turbulent flux partitioning (e.g., high correlation between R_n and both turbulent fluxes, and nearly aseasonal Bowen ratio values), (2) representation of canopy reflectance and emissivity (e.g., albedo's annual cycle showed significantly lower absolute values and greater than expected amplitudes), and (3) endogenous ecosystem or physiology-related seasonality (e.g., leaf-level stomatal and WUE dynamics driven by leaf ontogeny and demography). These processes are related to surface energy properties, canopy-atmosphere water dynamics, their interactions, and more importantly the coupling between energy carbon and water exchange. Here, we discuss some of our findings and suggest future observational and modeling work to improve simulations of tropical water and energy fluxes.

4.1 | Determinants and distribution of net radiation into turbulent fluxes

Observations showed ET to be driven by radiation rather than by moisture availability as predicted by models. The R_n was able to explain more than 60% of the 16-day LE values and although we report a low r^2 for the LE versus R_n regression at the southern forest of RJA, the coefficient of determination was driven by the low amplitude of the seasonal LE and R_n flux rather than the linear regressions not being able to predict LE.

Analysis of variability of the observed Bowen number annual cycle showed a nearly aseasonal ratio (~0.3 at the wet sites of K34 and CAX, and 0.21 at the dry sites K67 and RJA; Figure 4c). This suggests a proportional scaling of the forest's energy balance at each location (H was a constant fraction of LE). There was a relationship between the direction of bias in Bowen ratio estimates and site annual precipitation. LSMs overestimated dry-season Bowen values at the driest locations of K67 and RJA and underestimated the ratio at the wettest forests of K34 and CAX (models overestimated LE and underestimated H; similar to Best et al., 2015; Haughton et al., 2016; Morales et al., 2005). The expectation of a higher Bowen ratio (increase importance of H over LE) at the drier sites did not apply at these tropical forests and could be explained by: (1) LSMs had a negative bias in dry-season R_n. (2) Models underestimated dry-season LE, probably based on the incorrect assumption that water limitation (supply) rather than radiation (demand) drove the water flux (Federer, 1982). (3) LSMs may have difficulties simulating access to soil water at clay soils (e.g., K67) and although some recent model improvements have addressed this issue (e.g., ED2; see Longo, Knox, Levine, et al., 2019), measurements of field capacity and hydraulic conductivity were unavailable at our and other similar study sites. (4) To accurately estimate transpiration may require to include processes related to plant hydraulics, like the addition of stem-water and other additional storage terms (e.g., CLM5; see Yan et al., 2020). (5) The time of rainfall, precipitation intensity, and number of events (here we report significant differences among forest sites), rather than absolute precipitation values, may significantly influence the H/LE partition. Rainfall characteristics and forest canopy structure (see item 6) can be key in defining how much water would be intercepted (directly evaporated), drained, and/or infiltrated (stored and later supplied). (6) Models may be assuming excess E from leaves surfaces (e.g., because of the high LAI forest values) and not enough water would be reaching the soil for infiltration during the wet season. This "water deficit" would be carried out into the dry season, limiting the moisture available for transpiration and artificially increasing H.

4.2 | Representation of canopy reflectance (albedo) and thermal properties

Although significant, the differences between modeled-observed ET cannot be explained solely by the way models partition H and LE fluxes (Haughton et al., 2016). This study shows that correct

turbulent flux estimations require reliable R_n estimates. Most LSMs were able to capture the seasonal cycle of R_n. Thus, SW_{down} was provided to all models as a meteorological driver and dominated R_n. However, at CAX and RJA, both model LW_{out} and SW_{out} were higher than observations and consequently, seasonal values of R_n were underestimated. In some instances, the model-observation alignment was the result of obtaining the right answer for the incorrect reasons (e.g., LSMs overestimated SW_{out} and underestimated LW_{out} at K34). Models that consistently estimated higher than observed LW_{out} values may have to address the following issues: (1) the vegetation storage pool/heat capacity may be too low and/or (2) underestimated transpiration values, both causing T_{skin} to be too high. Additional measurements (e.g., thermal cameras, sapflow sensors, soil moisture profiles, and H_2O isotopes) would be necessary to measure T_{skin}, to infer the relationships between LE, H, and vegetation temperature, and to understand the mechanisms driving the relations between LW_{down} and LW_{out}.

Biases in LSM R_n can also be attributed to SW_{out} calculations. Observed low albedos did contrast with model simulations resulting in more reflective (brighter) forest surfaces. Models underestimated the amount of canopy-absorbed energy and may be imposing an "artificial" cooling effect. Surface albedo will be highly dependent on the leaf spectral properties and in general, canopy reflectance models attribute low albedos to high LAI values (e.g., PROSAIL [Féret et al., 2017] assumes albedos ~0.2 for a LAI>4) or albedos are parameterized as a constant (Hollinger et al., 2010). Nevertheless, we observed opposite sign regressions between LAI and albedo at CAX, thus indicating that α was not only driven by the quantity of leaves, but by leaf quality and vegetation reflective surfaces (e.g., wood and epiphylls; Chavana-Bryant et al., 2016; Wu et al., 2017). Across the Amazon, leaf phenology has shown to be a key driver of ET and carbon uptake (Albert et al., 2018; Chen et al., 2020; Manoli et al., 2018; Restrepo-Coupe et al., 2013; Wu et al., 2017) and should be incorporated/improved on the derivation of energy, radiation, and water fluxes, as well.

4.3 | Ecosystem characteristics and their contributions to water and energy flux seasonality

Our results showed that when H was higher than 20% LE, G_s reached a minimum of ~0.35 mmol m^{-2} s^{-1}, with no further reductions, indicating that the vegetation continued to transpire at the same or higher rate under relatively high Bowen ratio conditions. This finding may be not surprising as Stahl et al. (2013) found that during low precipitation periods 50% of a sample of 65 large tropical trees relied on soil water below 1 m depth, and others have reported hydraulic redistribution, stem-water storage, and additional processes that may explain forests' access to water during the dry season (Christoffersen et al., 2014; Oliveira et al., 2005; Yan et al., 2020). Moreover, the gradual dry-season decrease in G_s (as also reported in Christoffersen et al., 2014 and Costa et al., 2010) and increase in LE observed at the equatorial forests highlights the very significant role of evaporation during this period. However, only seasonal inventories of leaf age

and traits, and evaporation versus transpiration measurements (e.g., H and O isotopes) will offer models validation data to avoid misrepresentation of the plant water exchange (e.g., under/overestimating photosynthesis and WUE; Lawrence et al., 2007).

Leaf-level stomatal conductance (g_s) is expected to maximize carbon uptake while also reducing water loss from leaves (or reducing the carbon cost of hydraulic failure) when water is limiting (Anderegg et al., 2018; Medlyn et al., 2011; Sperry et al., 2017), and generally is site-specific and driven by adaptation to different atmospheric seasonal drivers (Brum et al., 2018). Ecosystem-level vegetation controls (e.g., LAI and leaf age and position across the canopy profile) determine the water flux, rate of photosynthesis, and the "acceptable" degree of water stress the forest can tolerate during the dry season (Albert et al., 2018; Restrepo-Coupe et al., 2013; Wu et al., 2017). Similar to G_s, at all four forests we observed contrasting degrees of seasonality in terms of WUE (with a range of ±25% of all year mean) and its timing metrics. Like GEP, across equatorial forests WUE increased as the dry season progressed and vice versa at RJA. At the ecosystem scale we found that the regression between WUE and G_s was not statistically significant at K34 and K67, negatively correlated at CAX and positively at RJA (Figure S22). The lack of a correlation between G_s and WUE would be driven by seasonal differences in intercellular CO_2 concentrations, atmospheric pressure and humidity, vegetation growth temperature, and other canopy characteristics (Lin et al., 2015; Medlyn et al., 2011, 2012). For example, higher vapor pressure deficit can increase transpiration and reduce WUE without any change in G_s and vice versa.

4.4 | Considerations for model improvement

This paper describes the seasonal patterns of different energy and water flux constituents and examines the relationships between them and different forest characteristics and climate variables at four tropical forests. We compared EC and biometric measurements to LSM simulations, as models represent our current understanding of the different atmosphere–biosphere processes at global and continental scales and are the ideal tool to predict vegetation responses to changes in climate. Our analysis highlights "forest phenology" as a significant driver of vegetation–atmosphere exchange and in particular, our data showed LSMs: (1) underestimated the amount of solar radiation the forests absorb and dry-season increases because we lack information regarding the relationship between leaf density and reflectance properties at high LAI values; (2) similarly, interception and direct evaporation may be overestimated at high LAI forests, and consequently LSMs may be underestimating infiltration and transpiration fluxes, overestimating canopy temperature, and consequently driving LSM output (3) to inaccurate estimations of LW_{out} (e.g., reducing the soil moisture content and increased canopy temperature would lead to unrealistically high T_{skin} and hence incorrect estimates of LW_{out}) and SW_{out} (e.g., if we incorrectly characterize forest structure, albedo will be too high). This seasonal bias on the outgoing flux (emissivity and albedo) dominated

the model-observation R_n differences and will have an effect in the estimation of H, LE fluxes, and the Bowen ratio. Our findings can be used to benchmark LSMs and develop more robust PFT parameterization. Improvements in model development will translate into better predictions of future surface–atmosphere exchange.

ORCID

Natalia Restrepo-Coupe https://orcid.org/0000-0003-3921-1772
Loren P. Albert https://orcid.org/0000-0002-9674-6071
Marcos Longo https://orcid.org/0000-0001-5062-6245
Ian Baker https://orcid.org/0000-0001-5162-1956
Naomi M. Levine https://orcid.org/0000-0002-4963-0535
David Galbraith https://orcid.org/0000-0002-5555-4823
Paul Moorcroft https://orcid.org/0000-0002-2876-4673
Scott R. Saleska https://orcid.org/0000-0002-4974-3628

REFERENCES

Abramowitz, G. (2005). Towards a benchmark for land surface models. *Geophysical Research Letters*, *32*(22). https://doi.org/10.1029/2005GL024419

Albert, L. P., Wu, J., Prohaska, N., de Camargo, P. B., Huxman, T. E., Tribuzy, E. S., Ivanov, V. Y., Oliveira, R. S., Garcia, S., Smith, M. N., Junior, R. C. O., Restrepo-Coupe, N., da Silva, R., Stark, S. C., Martins, G. A., Penha, D. V., & Saleska, S. R. (2018). Age-dependent leaf physiology and consequences for crown-scale carbon uptake during the dry season in an Amazon evergreen forest. *New Phytologist*, *219*(3), 870–884. https://doi.org/10.1111/nph.15056

Anderegg, W. R. L., Wolf, A., Arango-Velez, A., Choat, B., Chmura, D. J., Jansen, S., Kolb, T., Li, S., Meinzer, F. C., Pita, P., de Dios, V. R., Sperry, J. S., Wolfe, B. T., & Pacala, S. (2018). Woody plants optimise stomatal behaviour relative to hydraulic risk. *Ecology Letters*, *21*(7), 968–977. https://doi.org/10.1111/ele.12962

Aragão, L. E. O. C., Malhi, Y., Barbier, N., Lima, A., Shimabukuro, Y., Anderson, L., & Saatchi, S. (2008). Interactions between rainfall, deforestation and fires during recent years in the Brazilian Amazonia. *Philosophical Transactions of the Royal Society of London B: Biological Sciences*, *363*(1498), 1779–1785. https://doi.org/10.1098/rstb.2007.0026

Aragão, L. E. O. C., Malhi, Y., Roman-Cuesta, R. M., Saatchi, S., Anderson, L. O., & Shimabukuro, Y. E. (2007). Spatial patterns and fire response of recent Amazonian droughts. *Geophysical Research Letters*, *34*, 5. https://doi.org/10.1029/2006GL028946

Baker, I. T., Prihodko, L., Denning, A. S., Goulden, M., Miller, S., & da Rocha, H. R. (2008). Seasonal drought stress in the Amazon: Reconciling models and observations. *Journal of Geophysical Research*, *113*(G1), 1–10. https://doi.org/10.1029/2007JG000644

Baldocchi, D. D., Hincks, B. B., & Meyers, T. P. (1988). Measuring biosphere-atmosphere exchanges of biologically related gases with micrometeorological methods. *Ecology*, *69*(5), 1331–1340. https://doi.org/10.2307/1941631

Berry, J., Wolf, A., Campbell, J. E., Baker, I., Blake, N., Blake, D., Denning, A. S., Kawa, S. R., Montzka, S. A., Seibt, U., Stimler, K., Yakir, D., & Zhu, Z. (2013). A coupled model of the global cycles of carbonyl sulfide and CO_2: A possible new window on the carbon cycle. *Journal of Geophysical Research: Biogeosciences*, *118*(2), 842–852. https://doi.org/10.1002/jgrg.20068

Best, M. J., Abramowitz, G., Johnson, H. R., Pitman, A. J., Balsamo, G., Boone, A., Cuntz, M., Decharme, B., Dirmeyer, P. A., Dong, J., Ek, M., Guo, Z., Haverd, V., van den Hurk, B. J. J., Nearing, G. S., Pak, B., Peters-Lidard, C., Santanello, J. A., Stevens, L., & Vuichard, N. (2015). The plumbing of land surface models: Benchmarking model performance. *Journal of Hydrometeorology*, *16*(3), 1425–1442. https://doi.org/10.1175/JHM-D-14-0158.1

Best, M. J., Pryor, M., Clark, D. B., Rooney, G. G., Essery, R. L. H., Ménard, C. B., Edwards, J. M., Hendry, M. A., Porson, A., Gedney, N., Mercado, L. M., Sitch, S., Blyth, E., Boucher, O., Cox, P. M., Grimmond, C. S. B., & Harding, R. J. (2011). The Joint UK Land Environment Simulator (JULES), model description – Part 1: Energy and water fluxes. *Geoscientific Model Development*, *4*(3), 677–699. https://doi.org/10.5194/gmd-4-677-2011

Bonan, G. B. (2008). Forests and climate change: Forcings, feedbacks, and the climate benefits of forests. *Science*, *320*(5882), 1444–1449. https://doi.org/10.1126/science.1155121

Bony, S., Bellon, G., Klocke, D., Sherwood, S., Fermepin, S., & Denvil, S. (2013). Robust direct effect of carbon dioxide on tropical circulation and regional precipitation. *Nature Geoscience*, *6*(6), 447–451. https://doi.org/10.1038/ngeo1799

Brando, P. M., Goetz, S. J., Baccini, A., Nepstad, D. C., Beck, P. S. A., & Christman, M. C. (2010). Seasonal and interannual variability of climate and vegetation indices across the Amazon. *Proceedings of the National Academy of Sciences of the United States of America*, *107*(33), 14685–14690. https://doi.org/10.1073/pnas.0908741107

Brum, M., Vadeboncoeur, M. A., Ivanov, V., Asbjornsen, H., Saleska, S., Alves, L. F., Penha, D., Dias, J. D., Aragão, L. E. O. C., Barros, F., Bittencourt, P., Pereira, L., & Oliveira, R. S. (2018). Hydrological niche segregation defines forest structure and drought tolerance strategies in a seasonal Amazon forest. *Journal of Ecology*, *107*(1), 318–333. https://doi.org/10.1111/1365-2745.13022

Brutsaert, W. (1982). *Evaporation into the atmosphere: Theory, history and applications* (1st ed., Vol. *1*). Springer. https://www.springer.com/gp/book/9789027712479

Burba, G. (2010). *A brief practical guide to eddy covariance flux measurements: Principles and workflow examples for scientific and industrial applications*. LI-COR. https://www.licor.com/env/pdf/eddy_covariance/Brief_Intro_Eddy_Covariance.pdf

Chagnon, F. J. F., & Bras, R. L. (2005). Contemporary climate change in the Amazon. *Geophysical Research Letters*, *32*(13), L13703. https://doi.org/10.1029/2005GL022722

Chavana-Bryant, C., Malhi, Y., Wu, J., Asner, G. P., Anastasiou, A., Enquist, B. J., Cosio Caravasi, E. G., Doughty, C. E., Saleska, S. R.,

Martin, R. E., & Gerard, F. F. (2016). Leaf aging of Amazonian canopy trees as revealed by spectral and physiochemical measurements. *The New Phytologist*, *214*(3), 1049–1063. https://doi.org/10.1111/nph.13853

Chen, X., Maignan, F., Viovy, N., Bastos, A., Goll, D., Wu, J., Liu, L., Yue, C., Peng, S., Yuan, W., da Conceição, A. C., O'Sullivan, M., & Ciais, P. (2020). Novel representation of leaf phenology improves simulation of Amazonian evergreen forest photosynthesis in a land surface model. *Journal of Advances in Modeling Earth Systems*, *12*(1), e2018MS001565. https://doi.org/10.1029/2018MS001565

Christoffersen, B. O., Restrepo-Coupe, N., Arain, M. A., Baker, I. T., Cestaro, B. P., Ciais, P., Fisher, J. B., Galbraith, D., Guan, X., Gulden, L., van den Hurk, B., Ichii, K., Imbuzeiro, H., Jain, A., Levine, N., Miguez-Macho, G., Poulter, B., Roberti, D. R., Sakaguchi, K., ... Saleska, S. R. (2014). Mechanisms of water supply and vegetation demand govern the seasonality and magnitude of evapotranspiration in Amazonia and Cerrado. *Agricultural and Forest Meteorology*, *191*, 33–50. https://doi.org/10.1016/j.agrformet.2014.02.008

Clark, D. B., Mercado, L. M., Sitch, S., Jones, C. D., Gedney, N., Best, M. J., Pryor, M., Rooney, G. G., Essery, R. L. H., Blyth, E., Boucher, O., Harding, R. J., Huntingford, C., & Cox, P. M. (2011). The Joint UK Land Environment Simulator (JULES), model description – Part 2: Carbon fluxes and vegetation dynamics. *Geoscientific Model Development*, *4*(3), 701–722. https://doi.org/10.5194/gmd-4-701-2011

Costa, M. H., Biajoli, M. C., Sanches, L., Malhado, A. C. M., Hutyra, L. R., da Rocha, H. R., Aguiar, R. G., & de Araújo, A. C. (2010). Atmospheric versus vegetation controls of Amazonian tropical rain forest evapotranspiration: Are the wet and seasonally dry rain forests any different? *Journal of Geophysical Research, Biogeosciences*, *115*(G4). https://doi.org/10.1029/2009JG001179

da Rocha, H. R., Goulden, M. L., Miller, S. D., Menton, M. C., Pinto, L. D. V. O., de Freitas, H. C., & e Silva Figueira, A. M. (2004). Seasonality of water and heat fluxes over a tropical forest in eastern Amazonia. *Ecological Applications*, *14*(sp4), 22–32. https://doi.org/10.1890/02-6001

da Rocha, H. R., Manzi, A. O., Cabral, O. M., Miller, S. D., Goulden, M. L., Saleska, S. R., R.-Coupe, N., Wofsy, S. C., Borma, L. S., Artaxo, P., Vourlitis, G., Nogueira, J. S., Cardoso, F. L., Nobre, A. D., Kruijt, B., Freitas, H. C., von Randow, C., ... Maia, J. F. (2009). Patterns of water and heat flux across a biome gradient from tropical forest to savanna in Brazil. *Journal of Geophysical Research. Biogeosciences*, *114*(G1), G00B12. https://doi.org/10.1029/2007JG000640

Davidson, E. A., de Araújo, A. C., Artaxo, P., Balch, J. K., Brown, I. F., C. Bustamante, M. M., Coe, M. T., DeFries, R. S., Keller, M., Longo, M., Munger, J. W., Schroeder, W., Soares-Filho, B. S., Souza, C. M., & Wofsy, S. C. (2012). The Amazon basin in transition. *Nature*, *481*(7381), 321–328. https://doi.org/10.1038/nature10717

de Castanho, A. D. D. A., Galbraith, D., Zhang, K., Coe, M. T., Costa, M. H., & Moorcroft, P. (2016). Changing Amazon biomass and the role of atmospheric CO_2 concentration, climate, and land use. *Global Biogeochemical Cycles*, *30*(1), 18–39. https://doi.org/10.1002/2015GB005135

de Goncalves, L. G., Baker, I., Christoffersen, B., Costa, M., Restrepo-Coupe, N., da Rocha, H., & Saleska, S. (2009). *The large scale biosphere-atmosphere experiment in Amazônia, model intercomparison project (LBA-MIP) protocol*. ORNL-DAAC. https://daac.ornl.gov/LBA/guides/CD32_LBA_MIP_Drivers.html

Eva, H. D., & Huber, O. (Eds.). (2005). *A proposal for defining the geographical boundaries of Amazonia: Synthesis of the results from an Expert Consultation Workshop organized by the European Commission in collaboration with the Amazon Cooperation Treaty Organization—JRC Ispra, 7–8 June 2005*. Office for Official Publications of the European Communities.

Federer, C. A. (1982). Transpirational supply and demand: Plant, soil, and atmospheric effects evaluated by simulation. *Water Resources Research*, *18*(2), 355–362. https://doi.org/10.1029/WR018i002p00355

Féret, J.-B., Gitelson, A. A., Noble, S. D., & Jacquemoud, S. (2017). PROSPECT-D: Towards modeling leaf optical properties through a complete lifecycle. *Remote Sensing of Environment*, *193*, 204–215. https://doi.org/10.1016/j.rse.2017.03.004

Fisher, J. B., Huntzinger, D. N., Schwalm, C. R., & Sitch, S. (2014). Modeling the terrestrial biosphere. *Annual Review of Environment and Resources*, *39*(1), 91–123. https://doi.org/10.1146/annurev-environ-012913-093456

Fisher, R. A., Koven, C. D., Anderegg, W. R. L., Christoffersen, B. O., Dietze, M. C., Farrior, C. E., Holm, J. A., Hurtt, G. C., Knox, R. G., Lawrence, P. J., Lichstein, J. W., Longo, M., Matheny, A. M., Medvigy, D., Muller-Landau, H. C., Powell, T. L., Serbin, S. P., Sato, H., Shuman, J. K., ... Moorcroft, P. R. (2018). Vegetation demographics in Earth System Models: A review of progress and priorities. *Global Change Biology*, *24*(1), 35–54. https://doi.org/10.1111/gcb.13910

Fisher, R. A., Williams, M., Costa, D., Lola, A., Malhi, Y., Costa, D. F. R., Almeida, S., & Meir, P. (2007). The response of an Eastern Amazonian rain forest to drought stress: Results and modelling analyses from a throughfall exclusion experiment. *Global Change Biology*, *13*(11), 2361–2378. https://doi.org/10.1111/j.1365-2486.2007.01417.x

Foken, T. (2008). The energy balance closure problem: An overview. *Ecological Applications: A Publication of the Ecological Society of America*, *18*(6), 1351–1367.

Foken, T., Aubinet, M., & Leuning, R. (2012). The Eddy covariance method. In M. Aubinet, T. Vesala, & D. Papale (Eds.), *Eddy covariance* (pp. 1–19). Springer. https://doi.org/10.1007/978-94-007-2351-1_1

Foley, J. A., Prentice, I. C., Ramankutty, N., Levis, S., Pollard, D., Sitch, S., & Haxeltine, A. (1996). An integrated biosphere model of land surface processes, terrestrial carbon balance, and vegetation dynamics. *Global Biogeochemical Cycles*, *10*(4), 603–628. https://doi.org/10.1029/96GB02692

Freire, G. A. P., Ventura, D. J., Fotopoulos, I. G., Rosa, D. M., Aguiar, R. G., & de Araújo, A. C. (2020). Dinâmica de serapilheira em uma área de floresta de terra firme, amazônia ocidental. *Nativa*, *8*(3), 323–328. https://doi.org/10.31413/nativa.v8i3.9155

Fu, R., Yin, L., Li, W., Arias, P. A., Dickinson, R. E., Huang, L., Chakraborty, S., Fernandes, K., Liebmann, B., Fisher, R., & Myneni, R. B. (2013). Increased dry-season length over southern Amazonia in recent decades and its implication for future climate projection. *Proceedings of the National Academy of Sciences of the United States of America*, *110*(45), 18110–18115. https://doi.org/10.1073/pnas.1302584110

Getirana, A. C. V., Dutra, E., Guimberteau, M., Kam, J., Li, H.-Y., Decharme, B., Zhang, Z., Ducharne, A., Boone, A., Balsamo, G., Rodell, M., Toure, A. M., Xue, Y., Peters-Lidard, C. D., Kumar, S. V., Arsenault, K., Drapeau, G., Ruby Leung, L., Ronchail, J., & Sheffield, J. (2014). Water balance in the Amazon basin from a land surface model ensemble. *Journal of Hydrometeorology*, *15*(6), 2586–2614. https://doi.org/10.1175/JHM-D-14-0068.1

Gotangco Castillo, C. K., Levis, S., & Thornton, P. (2012). Evaluation of the new CNDV option of the community land model: Effects of dynamic vegetation and interactive nitrogen on CLM4 means and variability. *Journal of Climate*, *25*(11), 3702–3714. https://doi.org/10.1175/JCLI-D-11-00372.1

Goudriaan, J. (1986). A simple and fast numerical method for the computation of daily totals of crop photosynthesis. *Agricultural and Forest Meteorology*, *38*(1–3), 249–254. https://doi.org/10.1016/0168-1923(86)90063-8

Hagos, S., & Leung, L. R. (2011). On the relationship between uncertainties in tropical divergence and the hydrological cycle in global models. *Journal of Climate*, *25*(1), 381–391. https://doi.org/10.1175/JCLI-D-11-00058.1

Harper, A. B., Denning, A. S., Baker, I. T., Branson, M. D., Prihodko, L., & Randall, D. A. (2010). Role of deep soil moisture in modulating

climate in the Amazon rainforest. *Geophysical Research Letters*, 37(5). https://doi.org/10.1029/2009GL042302

Haughton, N., Abramowitz, G., Pitman, A. J., Or, D., Best, M. J., Johnson, H. R., Balsamo, G., Boone, A., Cuntz, M., Decharme, B., Dirmeyer, P. A., Dong, J., Ek, M., Guo, Z., Haverd, V., van den Hurk, B. J. J., Nearing, G. S., Pak, B., Santanello, J. A., … Vuichard, N. (2016). The plumbing of land surface models: Is poor performance a result of methodology or data quality? *Journal of Hydrometeorology*, 17(6), 1705–1723. https://doi.org/10.1175/JHM-D-15-0171.1

Held, I. M., & Soden, B. J. (2006). Robust responses of the hydrological cycle to global warming. *Journal of Climate*, 19(21), 5686–5699. https://doi.org/10.1175/JCLI3990.1

Hollinger, D. Y., Ollinger, S. V., Richardson, A. D., Meyers, T. P., Dail, D. B., Martin, M. E., Scott, N. A., Arkebauer, T. J., Baldocchi, D. D., Clark, K. L., Curtis, P. S., Davis, K. J., Desai, A. R., Dragoni, D., Goulden, M. L., Gu, L., Katul, G. G., Pallardy, S. G., Paw u, K. T., … Verma, S. B. (2010). Albedo estimates for land surface models and support for a new paradigm based on foliage nitrogen concentration. *Global Change Biology*, 16(2), 696–710. https://doi.org/10.1111/j.1365-2486.2009.02028.x

Jasechko, S., Sharp, Z. D., Gibson, J. J., Birks, S. J., Yi, Y., & Fawcett, P. J. (2013). Terrestrial water fluxes dominated by transpiration. *Nature*, 496(7445), 347–350. https://doi.org/10.1038/nature11983

Jin, M., & Liang, S. (2006). An improved land surface emissivity parameter for land surface models using global remote sensing observations. *Journal of Climate*, 19(12), 2867–2881. https://doi.org/10.1175/JCLI3720.1

Kato, S., Loeb, N. G., Rose, F. G., Doelling, D. R., Rutan, D. A., Caldwell, T. E., Yu, L., & Weller, R. A. (2012). Surface irradiances consistent with CERES-derived top-of-atmosphere shortwave and longwave irradiances. *Journal of Climate*, 26(9), 2719–2740. https://doi.org/10.1175/JCLI-D-12-00436.1

Keller, M., Alencar, A., Asner, G. P., Braswell, B., Bustamante, M., Davidson, E., Feldpausch, T., Fernandes, E., Goulden, M., Kabat, P., Kruijt, B., Luizão, F., Miller, S., Markewitz, D., Nobre, A. D., Nobre, C. A., Priante Filho, N., da Rocha, H., Silva Dias, P., … Vourlitis, G. L. (2004). Ecological research in the large-scale biosphere-atmosphere experiment in Amazonia: Early results. *Ecological Applications*, 14(4), S3–S16.

Kucharik, C. J., Foley, J. A., Delire, C., Fisher, V. A., Coe, M. T., Lenters, J. D., Young-Molling, C., Ramankutty, N., Norman, J. M., & Gower, S. T. (2000). Testing the performance of a dynamic global ecosystem model: Water balance, carbon balance, and vegetation structure. *Global Biogeochemical Cycles*, 14(3), 795–825. https://doi.org/10.1029/1999GB001138

Lawrence, D. M., Thornton, P. E., Oleson, K. W., & Bonan, G. B. (2007). The partitioning of evapotranspiration into transpiration, soil evaporation, and canopy evaporation in a GCM: Impacts on land-atmosphere interaction. *Journal of Hydrometeorology*, 8(4), 862–880. https://doi.org/10.1175/JHM596.1

Lee, J.-E., Oliveira, R. S., Dawson, T. E., & Fung, I. (2005). Root functioning modifies seasonal climate. *Proceedings of the National Academy of Sciences of the United States of America*, 102(49), 17576–17581. https://doi.org/10.1073/pnas.0508785102

Li, Y., Zhao, M., Motesharrei, S., Mu, Q., Kalnay, E., & Li, S. (2015). Local cooling and warming effects of forests based on satellite observations. *Nature Communications*, 6(1), 6603. https://doi.org/10.1038/ncomms7603

Lin, Y.-S., Medlyn, B. E., Duursma, R. A., Prentice, I. C., Wang, H., Baig, S., Eamus, D., de Dios, V. R., Mitchell, P., Ellsworth, D. S., de Beeck, M. O., Wallin, G., Uddling, J., Tarvainen, L., Linderson, M.-L., Cernusak, L. A., Nippert, J. B., Ocheltree, T. W., Tissue, D. T., … Wingate, L. (2015). Optimal stomatal behaviour around the world. *Nature Climate Change*, 5(5), 459–464. https://doi.org/10.1038/nclimate2550

Liou, K. N. (2002). *An introduction to atmospheric radiation*. International Geophysics (2nd ed., Vol. 84, pp. 1–583). Academic Press. https://www.sciencedirect.com/bookseries/international-geophysics/vol/84/suppl/C

Liu, Z., Ballantyne, A. P., & Cooper, L. A. (2019). Biophysical feedback of global forest fires on surface temperature. *Nature Communications*, 10(1), 214. https://doi.org/10.1038/s41467-018-08237-z

Longo, M., Knox, R. G., Levine, N. M., Alves, L. F., Bonal, D., Camargo, P. B., Fitzjarrald, D. R., Hayek, M. N., Restrepo-Coupe, N., Saleska, S. R., da Silva, R., Stark, S. C., Tapajós, R. P., Wiedemann, K. T., Zhang, K., Wofsy, S. C., & Moorcroft, P. R. (2018). Ecosystem heterogeneity and diversity mitigate Amazon forest resilience to frequent extreme droughts. *New Phytologist*, 219(3), 914–931. https://doi.org/10.1111/nph.15185

Longo, M., Knox, R. G., Levine, N. M., Swann, A. L. S., Medvigy, D. M., Dietze, M. C., Kim, Y., Zhang, K., Bonal, D., Burban, B., Camargo, P. B., Hayek, M. N., Saleska, S. R., da Silva, R., Bras, R. L., Wofsy, S. C., & Moorcroft, P. R. (2019). The biophysics, ecology, and biogeochemistry of functionally diverse, vertically and horizontally heterogeneous ecosystems: The Ecosystem Demography model, version 2.2 – Part 2: Model evaluation for tropical South America. *Geoscientific Model Development*, 12(10), 4347–4374. https://doi.org/10.5194/gmd-12-4347-2019

Longo, M., Knox, R. G., Medvigy, D. M., Levine, N. M., Dietze, M. C., Kim, Y., Swann, A. L. S., Zhang, K., Rollinson, C. R., Bras, R. L., Wofsy, S. C., & Moorcroft, P. R. (2019). The biophysics, ecology, and biogeochemistry of functionally diverse, vertically and horizontally heterogeneous ecosystems: The Ecosystem Demography model, version 2.2 – Part 1: Model description. *Geoscientific Model Development*, 12(10), 4309–4346. https://doi.org/10.5194/gmd-12-4309-2019

Lopes, A. P., Nelson, B. W., Wu, J., Graça, P. M. L. D. A., Tavares, J. V., Prohaska, N., Martins, G. A., & Saleska, S. R. (2016). Leaf flush drives dry season green-up of the Central Amazon. *Remote Sensing of Environment*, 182, 90–98. https://doi.org/10.1016/j.rse.2016.05.009

Manoli, G., Ivanov, V. Y., & Fatichi, S. (2018). Dry-season greening and water stress in Amazonia: The role of modeling leaf phenology. *Journal of Geophysical Research: Biogeosciences*, 123(6), 1909–1926. https://doi.org/10.1029/2017JG004282

Mauder, M., Genzel, S., Fu, J., Kiese, R., Soltani, M., Steinbrecher, R., Zeeman, M., Banerjee, T., Roo, F. D., & Kunstmann, H. (2018). Evaluation of energy balance closure adjustment methods by independent evapotranspiration estimates from lysimeters and hydrological simulations. *Hydrological Processes*, 32(1), 39–50. https://doi.org/10.1002/hyp.11397

Medlyn, B. E., Duursma, R. A., Eamus, D., Ellsworth, D. S., Prentice, I. C., Barton, C. V. M., Crous, K. Y., de Angelis, P., Freeman, M., & Wingate, L. (2012). Reconciling the optimal and empirical approaches to modelling stomatal conductance. *Global Change Biology*, 18(11), 3476–3476. https://doi.org/10.1111/j.1365-2486.2012.02790.x

Medlyn B. E., Duursma R. A., Eamus D., Ellsworth D. S., Prentice I. C., Barton C. V. M., Crous K. Y., Angelis P. D., Freeman M., & Wingate L. (2011). Reconciling the optimal and empirical approaches to modelling stomatal conductance. *Global Change Biology*, 17(6), 2134–2144. https://doi.org/10.1111/j.1365-2486.2010.02375.x

Medvigy, D., Wofsy, S. C., Munger, J. W., Hollinger, D. Y., & Moorcroft, P. R. (2009). Mechanistic scaling of ecosystem function and dynamics in space and time: Ecosystem demography model version 2. *Journal of Geophysical Research: Biogeosciences*, 114(G1), G01002. https://doi.org/10.1029/2008JG000812

Metcalfe, D. B., Meir, P., Aragão, L. E. O. C., Malhi, Y., da Costa, A. C. L., Braga, A., Gonçalves, P. H. L., de Athaydes, J., de Almeida, S. S., & Williams, M. (2007). Factors controlling spatio-temporal variation in carbon dioxide efflux from surface litter, roots, and soil organic matter at four rain forest sites in the eastern Amazon. *Journal of

Geophysical Research, 112(G4), 1–9. https://doi.org/10.1029/2007J G000443

Moderow, U., Aubinet, M., Feigenwinter, C., Kolle, O., Lindroth, A., Mölder, M., Montagnani, L., Rebmann, C., & Bernhofer, C. (2009). Available energy and energy balance closure at four coniferous forest sites across Europe. *Theoretical and Applied Climatology*, 98(3), 397–412. https://doi.org/10.1007/s00704-009-0175-0

Morales, P., Sykes, M. T., Prentice, I. C., Smith, P., Smith, B., Bugmann, H., Zierl, B., Friedlingstein, P., Viovy, N., Sabaté, S., Sánchez, A., Pla, E., Gracia, C. A., Sitch, S., Arneth, A., & Ogee, J. (2005). Comparing and evaluating process-based ecosystem model predictions of carbon and water fluxes in major European forest biomes. *Global Change Biology*, 11(12), 2211–2233. https://doi.org/10.1111/j.1365-2486.2005.01036.x

NASA/LARC/SD/ASDC. (2019). *CERES energy balanced and filled (EBAF) TOA and surface monthly means data in netCDF edition 4.1 [Data set]*. NASA Langley Atmospheric Science Data Center DAAC. https://doi.org/10.5067/TERRA-AQUA/CERES/EBAF_L3B.004.1

Oleson, K. W., Niu, G.-Y., Yang, Z.-L., Lawrence, D. M., Thornton, P. E., Lawrence, P. J., Stöckli, R., Dickinson, R. E., Bonan, G. B., Levis, S., Dai, A., & Qian, T. (2008). Improvements to the Community Land Model and their impact on the hydrological cycle. *Journal of Geophysical Research*, 113(G1), 1–26. https://doi.org/10.1029/2007J G000563

Oliveira, R. S., Dawson, T. E., Burgess, S. S. O., & Nepstad, D. C. (2005). Hydraulic redistribution in three Amazonian trees. *Oecologia*, 145(3), 354–363. https://doi.org/10.1007/s00442-005-0108-2

Peters, T. (2016). Water balance in tropical regions. In L. Pancel & M. Köhl (Eds.), *Tropical forestry handbook* (pp. 391–403). Springer. https://doi.org/10.1007/978-3-642-54601-3_40

Pitman, A. J. (2003). The evolution of, and revolution in, land surface schemes designed for climate models. *International Journal of Climatology*, 23(5), 479–510. https://doi.org/10.1002/joc.893

Powell, T. L., Galbraith, D. R., Christoffersen, B. O., Harper, A., Imbuzeiro, H. M. A., Rowland, L., Almeida, S., Brando, P. M., da Costa, A. C. L., Costa, M. H., Levine, N. M., Malhi, Y., Saleska, S. R., Sotta, E., Williams, M., Meir, P., & Moorcroft, P. R. (2013). Confronting model predictions of carbon fluxes with measurements of Amazon forests subjected to experimental drought. *New Phytologist*, 200(2), 350–365. https://doi.org/10.1111/nph.12390

Reed, D. E., Frank, J. M., Ewers, B. E., & Desai, A. R. (2018). Time dependency of eddy covariance site energy balance. *Agricultural and Forest Meteorology*, 249, 467–478. https://doi.org/10.1016/j.agrfo rmet.2017.08.008

Restrepo-Coupe, N., da Rocha, H. R., Hutyra, L. R., da Araujo, A. C., Borma, L. S., Christoffersen, B., Cabral, O. M. R., de Camargo, P. B., Cardoso, F. L., da Costa, A. C. L., Fitzjarrald, D. R., Goulden, M. L., Kruijt, B., Maia, J. M. F., Malhi, Y. S., Manzi, A. O., Miller, S. D., Nobre, A. D., von Randow, C., ... Saleska, S. R. (2013). What drives the seasonality of photosynthesis across the Amazon basin? A cross-site analysis of eddy flux tower measurements from the Brasil flux network. *Agricultural and Forest Meteorology*, 182–183, 128–144.

Restrepo-Coupe, N., Levine, N. M., Christoffersen, B. O., Albert, L. P., Wu, J., Costa, M. H., Galbraith, D., Imbuzeiro, H., Martins, G., da Araujo, A. C., Malhi, Y. S., Zeng, X., Moorcroft, P., & Saleska, S. R. (2017). Do dynamic global vegetation models capture the seasonality of carbon fluxes in the Amazon basin? A data-model intercomparison. *Global Change Biology*, 23(1), 191–208. https://doi.org/10.1111/gcb.13442

Rice, A. H., Pyle, E. H., Saleska, S. R., Hutyra, L. R., Palace, M., Keller, M., de Camargo, P. B., Portilho, K., Marques, D. F., & Wofsy, S. C. (2004). Carbon balance and vegetation dynamics in an old-growth Amazonian forest. *Ecological Applications*, 14(4), S55–S71.

Sellers, P. J. (1985). Canopy reflectance, photosynthesis and transpiration. *International Journal of Remote Sensing*, 6(8), 1335–1372. https://doi.org/10.1080/01431168508948283

Sena, E. T., Dias, M. A. F. S., Carvalho, L. M. V., & Dias, P. L. S. (2018). Reduced wet-season length detected by satellite retrievals of cloudiness over Brazilian Amazonia: A new methodology. *Journal of Climate*, 31(24), 9941–9964. https://doi.org/10.1175/JCLI-D-17-0702.1

Shuttleworth, W. J. (1988). Evaporation from Amazonian rainforest. *Proceedings of the Royal Society of London. Series B, Biological Sciences*, 233(1272), 321–346.

Silva Dias, M. A. F., Rutledge, S., Kabat, P., Silva Dias, P. L., Nobre, C., Fisch, G., Dolman, A. J., Zipser, E., Garstang, M., Manzi, A. O., Fuentes, J. D., Rocha, H. R., Marengo, J., Plana-Fattori, A., Sá, L. D. A., Alvalá, R. C. S., Andreae, M. O., Artaxo, P., Gielow, R., & Gatti, L. (2002). Cloud and rain processes in a biosphere-atmosphere interaction context in the Amazon Region. *Journal of Geophysical Research: Atmospheres*, 107(D20), 8072. https://doi.org/10.1029/2001JD000335

Sperry, J. S., Venturas, M. D., Anderegg, W. R. L., Mencuccini, M., Mackay, D. S., Wang, Y., & Love, D. M. (2017). Predicting stomatal responses to the environment from the optimization of photosynthetic gain and hydraulic cost. *Plant, Cell & Environment*, 40(6), 816–830. https://doi.org/10.1111/pce.12852

Spracklen, D. V., Baker, J. C. A., Garcia-Carreras, L., & Marsham, J. H. (2018). The effects of tropical vegetation on rainfall. *Annual Review of Environment and Resources*, 43(1), 193–218. https://doi.org/10.1146/annurev-environ-102017-030136

Stahl, C., Hérault, B., Rossi, V., Burban, B., Bréchet, C., & Bonal, D. (2013). Depth of soil water uptake by tropical rainforest trees during dry periods: Does tree dimension matter? *Oecologia*, 173(4), 1191–1201. https://doi.org/10.1007/s00442-013-2724-6

Stockli, R., Rutishauser, T., Dragoni, D., O'Keefe, J., Thornton, P., Jolly, M., Lu, L., & Denning, A. (2008). Remote sensing data assimilation for a prognostic phenology model. *Journal of Geophysical Research-Biogeosciences*, 113(G4). https://doi.org/10.1029/2008JG000781

Stoy, P. C., Katul, G. G., Siqueira, M. B. S., Juang, J.-Y., Novick, K. A., Uebelherr, J. M., & Oren, R. (2006). An evaluation of models for partitioning eddy covariance-measured net ecosystem exchange into photosynthesis and respiration. *Agricultural and Forest Meteorology*, 141(1), 2–18. https://doi.org/10.1016/j.agrformet.2006.09.001

Tan, Z.-H., Zhao, J.-F., Wang, G.-Z., Chen, M.-P., Yang, L.-Y., He, C.-S., Restrepo-Coupe, N., Peng, S.-S., Liu, X.-Y., da Rocha, H. R., Kosugi, Y., Hirano, T., Saleska, S. R., Goulden, M. L., Zeng, J., Ding, F.-J., Gao, F., & Song, L. (2019). Surface conductance for evapotranspiration of tropical forests: Calculations, variations, and controls. *Agricultural and Forest Meteorology*, 275, 317–328. https://doi.org/10.1016/j.agrformet.2019.06.006

Taylor, K. E. (2001). Summarizing multiple aspects of model performance in a single diagram. *Journal of Geophysical Research*, 106(D7), 7183–7192. https://doi.org/10.1029/2000JD900719

Trenberth, K. E., Fasullo, J. T., & Kiehl, J. (2009). Earth's global energy budget. *Bulletin of the American Meteorological Society*, 90(3), 311–324. https://doi.org/10.1175/2008BAMS2634.1

Wan, Z., Hook, S., & Hulley, G. (2015). MOD11A2 MODIS/terra land surface temperature/emissivity 8-day L3 global 1km SIN grid V006. *Distributed by NASA EOSDIS Land Processes DAAC*. https://doi.org/10.5067/MODIS/MOD11A2.006

Wehr, R., & Saleska, S. R. (2015). An improved isotopic method for partitioning net ecosystem–atmosphere CO_2 exchange. *Agricultural and Forest Meteorology*, 214–215, 515–531. https://doi.org/10.1016/j.agrformet.2015.09.009

Wehr, R., & Saleska, S. R. (2021). Calculating canopy stomatal conductance from eddy covariance measurements, in light of the energy budget closure problem. *Biogeosciences*, 18(1), 13–24. https://doi.org/10.5194/bg-18-13-2021

Wei, Z., Yoshimura, K., Wang, L., Miralles, D. G., Jasechko, S., & Lee, X. (2017). Revisiting the contribution of transpiration to global terrestrial evapotranspiration. *Geophysical Research Letters*, 44(6), 2792–2801. https://doi.org/10.1002/2016GL072235

Wilson, K., Goldstein, A., Falge, E., Aubinet, M., Baldocchi, D., Berbigier, P., Bernhofer, C., Ceulemans, R., Dolman, H., Field, C., Grelle, A., Ibrom, A., Law, B. E., Kowalski, A., Meyers, T., Moncrieff, J., Monson, R., Oechel, W., Tenhunen, J., … Verma, S. (2002). Energy balance closure at FLUXNET sites. *Agricultural and Forest Meteorology*, *113*(1–4), 223–243. https://doi.org/10.1016/S0168-1923(02)00109-0

Wofsy, S. C., Goulden, M. L., Munger, J. W., Fan, S.-M., Bakwin, P. S., Daube, B. C., Bassow, S. L., & Bazzaz, F. A. (1993). Net Exchange of CO_2 in a mid-latitude forest. *Science*, *260*, 1314–1317.

Worden, J., Noone, D., Bowman, K., Beer, R., Eldering, A., Fisher, B., Gunson, M., Goldman, A., Herman, R., Kulawik, S. S., Lampel, M., Osterman, G., Rinsland, C., Rodgers, C., Sander, S., Shephard, M., Webster, C. R., & Worden, H. (2007). Importance of rain evaporation and continental convection in the tropical water cycle. *Nature*, *445*(7127), 528–532. https://doi.org/10.1038/nature05508

Wu, J., Guan, K., Hayek, M., Restrepo-Coupe, N., Wiedemann, K. T., Xu, X., Wehr, R., Christoffersen, B. O., Miao, G., da Silva, R., de Araujo, A. C., Oliviera, R. C., Camargo, P. B., Monson, R. K., Huete, A. R., & Saleska, S. R. (2017). Partitioning controls on Amazon forest photosynthesis between environmental and biotic factors at hourly to interannual timescales. *Global Change Biology*, *23*(3), 1240–1257. https://doi.org/10.1111/gcb.13509

Yan, B., Mao, J., Dickinson, R. E., Thornton, P. E., Shi, X., Ricciuto, D. M., Warren, J. M., & Hoffman, F. M. (2020). Modelling tree stem-water dynamics over an Amazonian rainforest. *Ecohydrology*, *13*(1), e2180. https://doi.org/10.1002/eco.2180

Yanagi, S. N. M., & Costa, M. H. (2011). Simulations of tropical rainforest albedo: Is canopy wetness important? *Anais Da Academia Brasileira de Ciências*, *83*(4), 1171–1180. https://doi.org/10.1590/S0001-37652011005000047

SUPPORTING INFORMATION

Additional supporting information may be found online in the Supporting Information section.

How to cite this article: Restrepo-Coupe N, Albert LP, Longo M, et al. Understanding water and energy fluxes in the Amazonia: Lessons from an observation-model intercomparison. *Glob Change Biol*. 2021;27:1802–1819. https://doi.org/10.1111/gcb.15555